Solid Earth Discuss., https://doi.org/10.5194/se-2018-78
Manuscript under review for journal Solid Earth
Discussion started: 14 August 2018

Tectono-thermal evolution of Oman's Mesozoic passive continental margin under the obducting Semail Ophiolite: a case study Jebel Akhdar, Oman

Arne Grobe[1,2], Christoph von Hagke[1], Ralf Littke[2], István Dunkl[3], Franziska Wübbeler[1], Philippe Muchez[4], Janos L. Urai[1]

[1]Structural Geology, Tectonics, and Geomechanics, EMR Group, RWTH Aachen University, Germany
[2]Geology and Geochemistry of Petroleum and Coal, EMR Group, RWTH Aachen University, Germany
[3]Sedimentology & Environmental Geology, Geoscience Center Georg-August-Universität Göttingen, Germany
[4]Geodynamics and Geofluids Research Group, Department of Earth and Environmental Sciences, KU Leuven, Belgium

Correspondence to: Arne Grobe, arne.grobe@rwth-aachen.de, ORCID: 0000-0001-6471-0624

Keywords: basin modeling, passive margin, obduction, burial, Raman spectroscopy, thermochronology, thermal maturity

Abstract. The Mesozoic sequences of the Oman Mountains experienced only weak post-obduction overprint and deformation, thus they offer a unique natural laboratory to study obduction. We present a study of the pressure and temperature evolution in the passive continental margin under the Oman Ophiolite, using numerical basin models calibrated with thermal maturity data, fluid inclusion thermometry and low-temperature thermochronology.

Thermal maturity data from the Adam Foothills constrain burial in the foredeep moving in front of the advancing nappes to be at least 4 km. Peak temperature evolution in the carbonate platform under the ophiolite is only weakly dependent on the temperature of the overriding nappes which have cooled during transport from the oceanic subduction zone to emplacement. Fluid-inclusion thermometry yields pressure-corrected homogenization temperatures of 225 to 266 °C for veins formed during progressing burial, 296-364 °C for veins related to peak burial and 184 to 213 °C for veins associated with late-stage strike-slip faulting. In contrast, the overlying Hawasina nappes have not been heated above c. 170 ºC, as witnessed by only partial resetting of the zircon (U-Th)/He thermochronometer.

In combination with independently determined temperatures from solid bitumen reflectance, we infer that the fluid inclusions of peak-burial-related veins formed at minimum pressures of 225-285 MPa. This implies that the rocks of the future Jebel Akhdar Dome were buried under 8-10 km of ophiolite on top of 2 km of sedimentary nappes, which is in agreement with thermal maturity data of solid bitumen reflectance and Raman spectroscopy.

Burial of the passive margin under the ophiolite results in sub-lithostatic pore pressures, in agreement with observations on veins formed in dilatant fractures in the carbonates. We infer that overpressure is induced by rapid burial under the ophiolite nappes. Obduction-related tilt of the passive margin in combination with overpressure in the passive margin caused fluid migration towards the south in front of the nappes.

Exhumation of the Jebel Akhdar as indicated by our zircon (U-Th)/He data, integrated with existing data, started as early as the late Cretaceous to early Cenozoic, linked with extension along a major listric shear zone with top-to-NNE shear sense, together with an early phase of extensional dome formation. The carbonate platform and obducted nappes of the whole Jebel Akhdar cooled together below c. 170 °C between 50 and 40 Ma, before the final stage of anticline formation.

1. Introduction

The Permo-Mesozoic platform sediments of northern Oman (Figure 1; e.g. Beurrier et al., 1986; Glennie et al., 1974; Lippard et al., 1982) with hydrocarbon accumulations in the southern foreland of the Jebel Akhdar Dome (Figures 1 and 2) are overlain by the Semail ophiolite nappe complex, the largest and best-preserved ophiolite on Earth. Limited tectonic extension after obduction followed by uplift, folding and deep erosion and the present day arid climate formed exceptional exposures in three tectonic windows and in the foreland fold-and-thrust belt of the Oman Mountains (Figure 1). The Oman Mountains have been investigated in many studies focusing on tectonic history (Breton et al., 2004; Cooper et al., 2014; Glennie et al., 1973, 1974; Grobe et al., 2018; Loosveld et al., 1996; Searle, 2007), stratigraphic sequences (Van Buchem et al., 2002; Grelaud et al., 2006; Homewood et al., 2008), geodynamic modelling (Duretz et al., 2015), hydrocarbon source rocks (Van Buchem et al., 1996; Philip et al., 1995; Scott, 1990) and reservoir rocks (Arndt et al., 2014; De Keijzer et al., 2007; Koehrer et al., 2011; Virgo et al., 2013). Less well known is the temperature evolution of the sub-thrust sedimentary basin and the subsequent cooling history of the Jebel Akhdar (Aldega et al., 2017; Grobe et al., 2018; Hansman et al., 2017; Poupeau et al., 1998; Saddiqi et al., 2006). A better understanding of this would further constrain the dynamics of obduction.

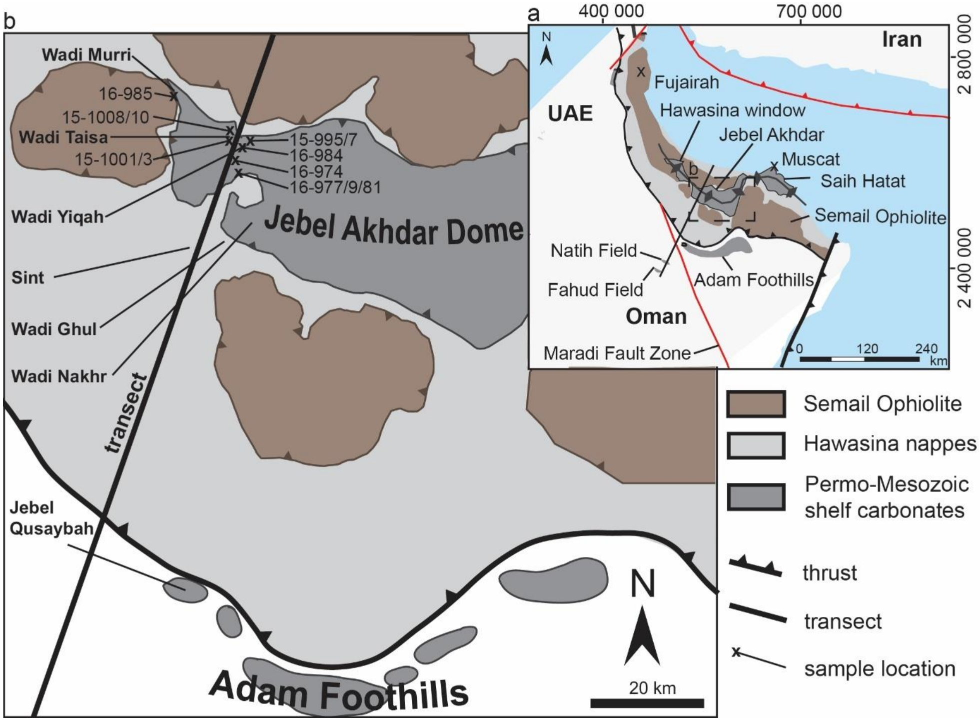

Figure 1: a) Tectonic setting of the Oman Mountains. Shaded in gray are the three tectonic windows of Hawasina, Jebel Akhdar and Saih Hatat as well as the Adam Foothills. Brown areas show the exposed Semail Ophiolite, black lines denote the obduction fronts of Semail and Masirah ophiolites, red lines denote lithosphere-scale structures. The modeled transect (black line) crosscuts the Jebel Akhdar window and continues to the Natih and Fahud oil fields in the southwestern mountain foreland. b) Geologic map of the Jebel Akhdar window with the location of the modeled transect (solid black line) and the locations of thermal maturity data (x).

The full Permo-Mesozoic sequence of the carbonate platform below the ophiolite is well exposed, providing outcrop samples to study the pressure and temperature history of this rapidly buried passive-margin sequence. In other orogens, peak temperatures related to nappe emplacement were reconstructed by analyzing thermal maturity of finely dispersed organic material (e.g. Teichmüller and Teichmüller, 1986; Eastern Alps: Lünsdorf et al., 2012; Southern Alps: Rantitsch and Rainer, 2003; Apennines: Reutter et al., 1988). However, the number of studies of thermal and pressure effects on overthrust sedimentary basins is limited and modeling approaches to reconstruct such large scale overthrusts are rare (e.g. Deville and Sassi, 2006; Ferreiro Mählmann, 2001; Oxburgh and Turcotte, 1974; Roure et al., 2010; Wygrala, 1989). In these studies, a main difficulty is to differentiate between temperature history of obduction and overprinting by later phases of orogeny. In the Oman Mountains, peak temperatures reached by obduction have not been overprinted, and fluid migration in the thrust belt is predominantly related to obduction.

In this paper we present new thermal maturity, thermochronology and fluid inclusion data, and model the pressure-temperature evolution of a transect across the entire Jebel Akhdar extending from the undeformed passive margin sequence in the south to the Batinah coast in the north (Figure 2). This allows to better constrain temperature and pressure conditions of deepest burial as well as the time of dome formation and exhumation which is linked to the structural and tectonic evolution of the area.

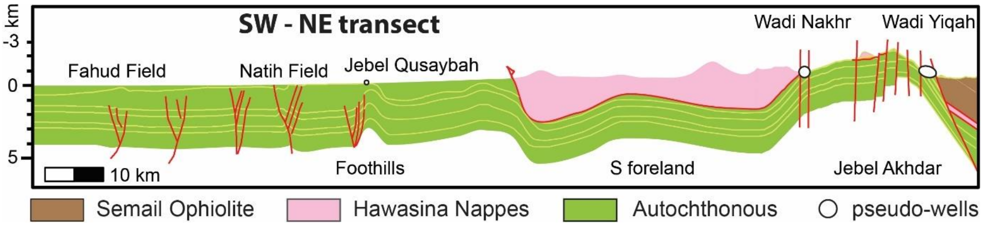

Figure 2: Structural transect used for modeling of the Jebel Akhdar Dome and its southern foreland (compiled from Al-Lazki et al., 2002; Filbrandt et al., 2006; Searle, 2007; Warburton et al., 1990). Highlighted are the locations of the pseudo-wells (white circles, size depict area of sample interpolation) in Wadi Nakhr, Wadi Yiqah and at Jebel Qusaybah, Adam Foothills, which were used for model calibration.

2. Geological setting

2.1. Tectonic setting

Along the northeastern coast of Arabia, the NW-SE oriented Oman Mountains form a more than 400 km long anticlinal orogen (Figure 1). The mountain belt consists of allochthonous sedimentary and ophiolitic nappes thrust onto a Permo-Mesozoic passive continental margin (Breton et al., 2004; Glennie et al., 1973; Loosveld et al., 1996; Searle and Cox, 2002).

This margin was formed during opening of the Neotethyan ocean (e.g. Loosveld et al., 1996) and the Permo-Mesozoic Hawasina Basin (Béchennec et al., 1988; Bernoulli et al., 1990). Cretaceous convergence of Arabia and Iran inverted the rifting and initiated subsea thrusting of the later Semail Ophiolite on top of the Arabian Plate at 97-92 Ma, as recorded by U-Pb geochronology (Rioux et al., 2013, 2016; Warren et al., 2005) and ^{40}Ar/^{39}Ar dating of the metamorphic sole (Hacker et al., 1996). Obduction initiation and the advancing ophiolite resulted in a flexural forebulge that moved southwestwards through the passive margin during the Upper Cretaceous

(Robertson, 1987). Forebulge migration induced up to 1100 m of uplift of the Permo-Mesozoic Arabian Platform and erosion of the Cretaceous platform sediments (Searle, 2007). In the field this can be observed at the Wasia-Aruma Break (e.g. Robertson, 1987).

During northeastward directed subduction of the Arabian margin, parts of the Hawasina ocean sediments and volcanics detached and became accreted in front and beneath the ophiolite nappe (Béchennec et al., 1988, 1990; Glennie et al., 1974; Searle et al., 2003; Warburton et al., 1990). Palinspastic reconstructions of the Hawasina Nappes locate the position of the initial ophiolite thrusting 300-400 km offshore the Arabian coast (Béchennec et al., 1988; Glennie et al., 1974).

Burial under the allochthonous sequences led to the formation of three crack-seal calcite vein generations in the margin sequence, which represent overpressure build-ups and releases (Gomez-Rivas et al., 2014; Grobe et al., 2018; Hilgers et al., 2006; Holland et al., 2009; Virgo, 2015). Peak metamorphism of the subducted margin is recorded by eclogites exposed in the As Sifah region (E-Saih Hatat, Figure 1a), where the burial triggered thermal climax resulted in zircon and rutile recrystallization at c. 79 Ma (Warren et al., 2003).

The sedimentary record in the Batinah coast and the foreland, as well as laterite formation on top of the ophiolite suggest that obduction slowed or stopped in the early Paleogene, and the ophiolite was exposed subaerially (Coleman, 1981; Forbes et al., 2010; Nolan et al., 1990). This slowdown might relate to the formation of the Makran subduction zone at c. 35 Ma (Figure 1; Agard et al., 2005; Hassanzadeh and Wernicke, 2016; Jacobs et al., 2015; Mouthereau, 2011). This shift of deformation to the north resulted in preservation of the initial stage of the obduction orogen in northern Oman.

Regional post-obduction extension took place along ductile top-to-NNE shear zones, dated to 64±4 Ma (Hansman et al., 2018), followed by NW-SE striking normal fault systems (Al-Wardi and Butler, 2007; Fournier et al., 2006; Grobe et al., 2018; Hanna, 1990; Hilgers et al., 2006; Holland et al., 2009; Loosveld et al., 1996; Mattern and Scharf, 2018; Virgo, 2015). Renewed Arabia-Eurasia convergence during the Cenozoic formed the three dome structures with the associated tectonic windows. Timing of formation and exhumation of the Jebel Akhdar Dome is still debated. Stratigraphic arguments for a late Cretaceous doming are Maastrichtian rocks unconformably deposited on Hawasina (Bernoulli et al., 1990; Fournier et al., 2006; Hanna, 1990; Nolan et al., 1990), while inclined Miocene strata at the northern fringes of the dome points to a younger Miocene doming (Glennie et al., 1973). Consequently, some models suggest a two-phased exhumation in Cretaceous and Miocene (Searle, 1985, 2007), in agreement with structural observations suggesting early dome formation and later amplification of the structure (Grobe et al., 2018).

Thermochronological constraints for the exhumation of the Jebel Akhdar Dome from samples below and above the carbonate platform were reported (Hansman et al., 2017; Mount et al., 1998; Poupeau et al., 1998; Saddiqi et al., 2006). Earlier studies argue for two-stage cooling with reheating in late Miocene (Poupeau et al., 1998; Saddiqi et al., 2006). More recent studies, however, have shown that the data of Poupeau et al. (1998) and Saddiqi et al. (2006) can also be explained by a cooling-only scenario with exhumation in the Eocene (Hansman et al., 2017).

2.2. Stratigraphic sequence

Sediments in the Jebel Akhdar area consist of a pre-Permian sequence (Autochthonous A, Figure 3) unconformably overlain by a Permo-Mesozoic sequence (Autochthonous B, Figure 3; Beurrier et al., 1986; Breton et al., 2004; Glennie et al., 1974; Rabu et al., 1990). During the late Cretaceous, Hawasina nappes and the Semail Ophiolite were emplaced onto the passive margin, and neo-autochthonous rocks of Cenozoic age were deposited on top of the ophiolite after obduction (Béchennec et al., 1988; Forbes et al., 2010; Loosveld et al., 1996).

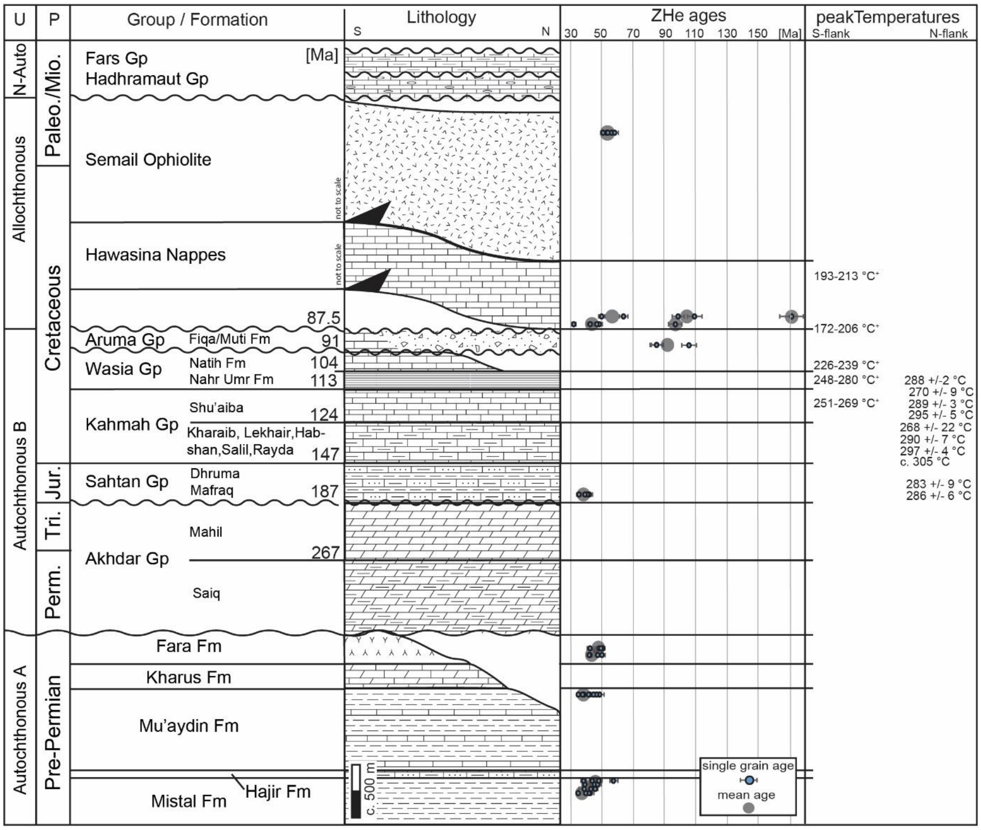

Figure 3: Stratigraphy of the Jebel Akhdar area with its two passive margin sequences Autochthonous A and B overthrust by Hawasina and Semail Nappes and unconformably overlain by neo-autochthonous units (Figure 1). Ages (Forbes et al. 2010) are basin modeling input data. In addition, thermal calibration data is shown: ZHe ages (Table 2) show two different grain age populations. Maximum burial temperatures from organic matter maturity (black, Table 1) outline the temperature increase with stratigraphic age. Temperature data was supplemented by values from *Mozafari et al. (2015) and $^+$Grobe et al. (2016). (U = Unit, P =Period). Note that the Semail and Hawasina nappes are shown in their structural rather than stratigraphic positions. Data is compiled from Beurrier et al. (1986), Loosveld et al. (1996), Terken et al. (2001) and Forbes et al. (2010).

Autochthonous A deposits are exposed in the Jebel Akhdar window down to the Mistal Fm. (Beurrier et al., 1986). Black limestones of the Hajir Fm., mudstone rich carbonate beds of the Mu'aydin Fm. and lime- and dolostones of the Kharus Fm. conformably overlie the Mistal Fm. (Beurrier et al., 1986; Glennie et al., 1974). Platform break-up is recorded by laminated cherts and volcanoclastics of the Fara Fm. (Beurrier et al., 1986) followed by an unconformity representing a gap from Cambrian to Permian times (Loosveld et al., 1996). After establishment of the Neotethyan Ocean during the Permian, northern Oman returned to stable passive margin conditions and the carbonate platform of the Autochthonous B developed, with the Akhdar Gp. at its base (Koehrer et al., 2010; Pöppelreiter et al., 2011). This is unconformably overlain by limestones with clastic interlayers of the Jurassic Sahtan Gp. (Beurrier et al., 1986; Pratt et al., 1990). Limestones with marly, frequently organic-rich intercalations of the Cretaceous Kahmah (Habsi et al., 2014; Vahrenkamp, 2010) and Wasia groups (Grelaud et al., 2006;

Homewood et al., 2008; Philip et al., 1995) form the youngest platform sediments (Robertson, 1987; Warburton et al., 1990).

The obduction-related moving forebulge and associated uplift ended passive margin deposition and eroded the topmost Wasia Gp. (Natih Fm.) in the Jebel Akdhar (Figure 3), and deeper in the Saih Hatat region. Deposition in the foredeep basins in front and behind the forebulge was dominated by the syn- and postorogenic, conglomerate-rich sediments of the Muti Fm., Aruma Gp. (Beurrier et al., 1986; Robertson, 1987). Towards the south, in the Adam Foothills, this laterally grades to calcareous foreland sediments of the Fiqa Fm. (Forbes et al., 2010; Robertson, 1987; Warburton et al., 1990).

Hawasina sediments accreted in front and beneath the ophiolite represent marine slope and basin facies, time equivalent to the Autochthonous B (Béchennec et al., 1990). After obduction of oceanic crust on top of the passive margin, neo-autochthonous evaporites and carbonates of the Paleocene to Eocene Hadhramaut Gp. and bivalve-rich dolomites and limestones of the Oligo- to Pliocene Fars Gp. were deposited south of the mountains (Béchennec et al., 1990; Forbes et al., 2010). Paleogeographical reconstructions show the Oman Mountains had high relief after obduction, followed by a low relief landscape until the early Eocene (Nolan et al., 1990). In the middle Eocene marine transgression caused widespread deposition of limestones, as witnessed e.g. by the Seeb and Ruwaydah Formations (Nolan et al., 1990). Post Eocene times show renewed relief development and continued uplift until recent times (Glennie et al., 1974; Searle, 2007).

2.3. Temperature evolution of the Autochthon

Only limited paleo-temperature data is available from the carbonate platform. Peak-burial temperatures of 226-239 °C for the top of the platform were measured using solid bitumen reflectance and Raman spectroscopy of carbonaceous material (RSCM) in the Jebel Akhdar (Grobe et al., 2016). Vein crystallization temperatures of 166-205 °C at the top of the Natih A (near Al Hamra) were measured by quartz-calcite thermometry in veins formed during ophiolite-induced burial (Gen. III of Grobe et al., 2018), and approximately 255 °C for veins associated with a later normal fault network (Gen V of Grobe et al., 2018; Stenhouse, 2014). Fluid inclusions (FI) of bedding parallel pinch-and-swell veins (top-to-NNE shear after peak burial, Gen. IV of Grobe et al., 2018) show uncorrected minimum trapping temperatures of 134-221 °C in the lower beds of the Sahtan Group at Wadi Nakhr (Holland et al., 2009). Reflectance measurements of solid-bitumen-containing veins in the Wadi Ghul (Gen I of Grobe et al., 2018), which are interpreted to be associated with fluid mobilization during forebulge migration, showed maximum temperatures of 230 °C (Fink et al., 2015).

Reconstructions of the thermal history using numerical basin modeling were presented for the southern foreland and the contained Natih Fm. outlining its extreme efficiency interpreted to be a result of thrusting-induced lateral migration (Terken, 1999; Terken et al., 2001) and the Proterozoic hydrocarbon source rocks (Visser, 1991).

2.4. Temperature evolution of the Semail Ophiolite nappe / Allochthon

Initial intra-oceanic ophiolite thrusting and associated metamorphism at its sole took place at peak temperatures of 840 ± 70 °C at 97-92 Ma measured at several locations in the Oman Mountains (Gnos and Peters, 1993; Hacker and Mosenfelder, 1996; Rioux et al., 2013; Searle and Cox, 2002; Warren et al., 2003). At 90-85 Ma the base of the ophiolite cooled to 350 ± 50 °C (white mica Ar/Ar dating, Gnos and Peters, 1993). At around 80 Ma the deepest burial of the Oman margin beneath the ophiolite was reached (Hacker and Mosenfelder, 1996; Warren et al., 2005) with temperatures in the metamorphic sole below 300 °C (Le Metour et al., 1990; Saddiqi et al., 2006). Due to the at least 2 km thick imbricated Hawasina Nappes between the ophiolite and the passive margin sequence, the thermal overprint of the nappe temperature on the top of the carbonate platform was low. Limited thermal overprinting of the units underlying the ophiolite is supported by the fact that the sediments of the nappes directly below the ophiolite do not show signs of regional metamorphism in the Jebel Akhdar region (Searle, 1985). A lithospheric scale thermo-mechanical model of the thrusting in northwestern Oman includes a thermal anomaly c. 100 km northwest offshore the Arabian margin to initiate subsea thrusting (Duretz et al. 2015).

2.5. Petroleum system elements

Several petroleum systems developed in the carbonate platform of northern Oman with important source rock horizons in the Natih Fm. (Natih Members B and E). Both members contain Type I/II kerogen with total organic carbon contents up to 15 % in the Natih B and up to 5 % in the Natih E, respectively (Terken, 1999). Ophiolite obduction in northern Oman led to over-mature Natih source rocks (Grobe et al., 2016). However, the thermal impact of the moving forebulge and the importance of tectonic processes for fluid migration below and in front of the obduction orogen are not clear. At least three different generations of solid bitumen particles in veins and source rocks on the southern slope of the Jebel Akhdar suggest pulses of hydrocarbon generation and migration in front of the Oman Mountains (Fink et al., 2015; Grobe et al., 2016). In central Oman, Shu'aiba and Tuwaiq oils are produced out of Kahmah and Sahtan Gp. reservoirs, sealed by argillaceous shales of the Nahr Umr Fm. (Terken et al., 2001). These units are all well-exposed in the Oman Mountains.

3. Methods

Samples for thermal reconstruction were collected during several field campaigns between 2013 and 2016 in the Jebel Akhdar Dome (Figure 2).

3.1. Elemental analysis and thermal maturity

To determine thermal maturity, over 100 dark, unweathered and organic-rich samples were taken from different stratigraphic units in the Jebel Akhdar (Figure 3). Based on total organic carbon (TOC) content as determined by Grobe et al., (2016), 13 samples were selected for thermal maturity analysis on surfaces cut perpendicular to bedding. Results were used to calibrate peak-burial temperatures of the numerical basin models. The organic particles lack sufficient size or surface quality for reflectance measurements and are therefore investigated by confocal Raman spectroscopy of carbonaceous material. The technique measures vibrational energies of chemical bonds which change during temperature induced reorganization of amorphous carbonaceous material (kerogen) to graphite (e.g. Aoya et al., 2010; Beyssac et al., 2002; Kouketsu et al., 2014). Measurements were conducted at the Geoscience Center, Göttingen, on a Horiba Jobin Yvon HR800 UV spectrometer attached to an Olympus BX-41 microscope and a 100× objective. A high-power diode laser with a wavelength of 488 nm and an output power of 50 mW was installed and a D1 filter avoided sample alteration by heating. Each spectral window (center at 1399.82 cm^{-1}, grid of 600 lines/mm) was measured 5 to 10 times for 2 to 10 seconds with a Peltier CCD detector at activated intensity correction. For quality control, the 520.4 cm^{-1} line of a Si-wafer was measured every 30 minutes without observable drift of the measurements. To transform the measured data into VR_r values the scaled total area (STA) approach of Lünsdorf (2016) was applied with the equation of Grobe et al. (2016):

$$VR_r = -\frac{STA - 280.13}{24.71} \quad [\%]$$

From VR_r calculations peak-burial temperatures were determined following the approach of Barker and Pawlewicz (1994). For calibration of the numerical basin models, data was supplemented by thermal maturity and peak-burial temperature data of 63 Natih B source rock samples, taken around the Jebel Akhdar Dome (Grobe et al., 2016), and two data points in the Adam Foothills on Jebel Qusaybah (Mozafari et al., 2015).

3.2. Fluid inclusion thermometry

Doubly-polished wafers (c. 200 µm thick) of four vein samples (FI-N1, -N2, -M1, -M2) have been prepared according to the procedure described by Muchez et al. (1994). Fluid inclusion (FI) petrography and thermometry was performed to analyze the temperature-pressure conditions and fluid's salinity. FIs represent paleofluids accidentally trapped in a crystalline or amorphous solid during mineralization, lithification or both (Diamond, 2003). If unaffected by later changes, trapping pressure and temperature is given by the homogenization temperature (Barker and Goldstein, 1990). Based on the time of trapping primary (mineral growth), secondary (fracture-related) and pseudosecondary inclusions are distinguished (Barker and Goldstein, 1990; Diamond, 2003; Goldstein, 2001; Van Den Kerkhof and Hein, 2001):

Two calcite vein samples of the Natih Fm. (FI-N1 and 2, Locations Figure 4) represent conditions related to early burial (FI-N2, structural generation I of Grobe et al. 2018), and burial beneath the ophiolite (FI-N1, structural generation III of Grobe et al. 2018). Two quartz-rich calcite veins of the Muti Fm. (FI-M1 and 2, Locations Figure 4) are related to late, NE-SW striking strike slip faults (generation IX of Grobe et al. 2018). FI assemblages were defined and fluid inclusions measured with a Linkam THMSG600 thermostage (accuracy ± 0.1 °C) attached to an Olympus BX60 microscope at the KU Leuven, Belgium. Calibration was performed using CO_2, H_2O-NaCl, H_2O-KCl, and H_2O standards. Homogenization temperatures (T_h) were measured prior to temperatures of complete freezing (T_f), first melt (T_{fm}), and complete melting of ice ($T_{m(ice)}$) to avoid stretching or leakage due to the volume increase during ice formation. All measured temperatures were recorded during heating, except of the freezing temperature (T_f). Pressure corrections of T_h were conducted with the program FLINCOR (Brown, 1989) for 280 and 340 MPa, assuming 8 to 10 km of ophiolite overburden (see model results, ρ= c. 3070 kg/m³) and 2 km of sedimentary Hawasina Nappes (ρ= c. 2450 kg/m³), and for 45 MPa, assuming 2°km of sedimentary overburden (Al-Lazki et al., 2002; Grobe et al., 2016). Fluid salinities were calculated from the $T_{m(ice)}$ values considering a H_2O-NaCl composition (Bodnar, 1993), which is based on the T_{fm} values.

3.3. Thermochronology

Zircon (U-Th)/He (ZHe) dating allows to reconstruct the tectono-thermal history of the topmost few kilometers of the Earth's crust. Helium retention in less metamict zircon crystals is sensitive in the temperature range between c. 130 and 170 °C, i.e. the zircon partial retention zone (PRZ, Reiners, 2005). 11 rocks sampled above, below and within the carbonate platform were selected for ZHe dating. Zircon crystals were released using high voltage pulse crushing (http://www.selfrag.com) and concentrated by standard mineral separation processes (drying, dry sieving, magnetic and heavy liquid separation). Three to eight clear, intact, euhedral single crystals were selected per sample and transferred into platinum micro-capsules. They were degassed under high vacuum by heating with an infrared diode and extracted gas purified using a SAES Ti-Zr getter at 450 °C. Helium was analyzed with a Hiden triple-filter quadrupole mass spectrometer. Degassed zircons were subsequently dissolved in pressurized teflon bombs, spiked and U, Th and Sm measured with a Perkin Elmer Elan DRC II ICP-MS equipped with an APEX micro flow nebulizer.

Time-temperature histories were reconstructed using the HeFTy 1.8.3 software package (Ketcham, 2005) applying kinetic zircon properties of Guenther et al. (2013). For samples with reset zircons the only constraint used was a minimum temperature above 200 °C between deposition and the calculated ZHe age. Thermal modeling was conducted until 100 statistically good time-temperature paths were achieved (goodness of fit: 0.5, value for acceptable fit: 0.05). In cases where this was not possible, at least 10,000 independent paths were calculated.

3.4. Numerical basin modeling

Structural evolution was palinspastically reconstructed starting from the present-day profile using Move 2D (2016.1, Midland Valley Exploration). Geometries and relative ages of the structures were supplemented with subsurface data (Al-Lazki et al., 2002; Filbrandt et al., 2006; Searle et al., 2004; Warburton et al., 1990). The reconstruction workflow was as follows: (1) faulted layers in the southern foreland were restored, (2) doming was retro-deformed by vertical simple shear, before (3) normal faults in the Jebel Akhdar were restored. This sequence is based on our tectonic model (Grobe et al., 2018). The resulting geometries were used as input for 2D PetroMod 2014.1 (Schlumberger) basin modeling, enabling thermal maturity reconstruction for vitrinite reflectance values of 0.3 to 4.7 % by the use of the EASY % R_0 approach (Sweeney and Burnham, 1990). The numerical basin model is based on a conceptional definition of events. Based on this sequence of events (sedimentation, erosion, hiatus) a forward, event-stepping modeling is performed, starting with the deposition of the oldest layer. For each event lithologies and related petrophysical rock properties are assigned. The final basin model (representing the present day) fits the geometries deduced from seismic interpretation and geology. This is the first time that ophiolite obduction is reconstructed using a petroleum system modelling software such as PetroMod. To simulate obduction we used a rapid, stepwise-laterally-advancing emplacement, i.e. sedimentation, of ophiolitic rocks. This is reasonable, as we will show that the ophiolite did not thermally overprint the passive margin sequence from above. For our conceptual model the following sequence of events was implemented (Figure 3): (1) passive margin carbonate sedimentation from Permian until late Cenomanian times (Forbes et al., 2010; Loosveld et al., 1996), interrupted by a short erosional period at the Triassic-Jurassic boundary (Koehrer et al., 2010; Loosveld et al., 1996), (2) a moving forebulge associated with a paleo-water depth increase in its foredeep and erosion of the top of the carbonate platform in the north of the transect (Wasia-Aruma break, 91-88.6 Ma, Robertson, 1987), (3) the emplacement of allochthonous sedimentary nappes and (4) subsequent obduction, i.e. stepwise, rapid sedimentation, of the ophiolite with deepest burial reached at c. 79 Ma (Warren et al., 2005). The area of the Adam Foothills, represented in the transect by the Jebel Qusaybah, is a relic of the moving forebulge not overthrust by allochthonous units – this was used to calibrate burial depth of the foredeep at this point in the transect. The south of the foothills is unaffected by foredeep and obduction, but also lacks thermal calibration data. Absolute ages, thicknesses, lithologies and related petrophysical properties as well as source rock properties were associated according to results of our own field mapping and the compiled data from Forbes et al. (2010; Figure S1).

Thermal boundary conditions of the model have been defined for each time step by the basal heat flow (HF) and the sediment water interface temperature (SWIT), representing the upper thermal boundary (Figure S2). To account for active margin tectonics and uplift and exhumation of the Jebel Akhdar, we assume an increase in basal heat flow since the late Cretaceous. The resulting heat flow trend (Figure S2, Terken et al., 2001; Visser, 1991) has been assigned to the entire transect. Paleo-surface temperatures were estimated based on Oman's paleo-latitude (after Wygrala, 1989) corrected by the effect of the paleo-water depth (PWD) derived from the facies record (Van

Buchem et al., 2002; Immenhauser et al., 1999; Immenhauser and Scott, 2002; Koehrer et al., 2010; Pratt et al., 1990; Robertson, 1987).

This set-up has been iterated until modeling results fit the thermal calibration data (Table 1). Main uncertainties derive from the unknown thickness of paleo-overburden (Muti Fm., Ophiolite, Hawasina Nappes) and uncertainty of paleo-basal heat flow. Present-day heat flow was calibrated by data and borehole temperatures of Visser (1991) and Rolandone et al. (2013) and peak-burial temperatures determined by Raman spectroscopy and solid bitumen reflectance data (Table 1). From surface samples and their position in the stratigraphic column various pseudo-wells were created (e.g. Nöth et al., 2001) and used as control points for the 2D model (Figure 2). The model was used for sensitivity analyses of different input parameters.

4. Results

4.1. Thermal maturity and host rock burial temperatures

From Raman spectroscopy, integrated deformation peaks (D-peaks) give scaled total areas of 90-156 which correspond to peak-burial temperatures of 266 to 300 °C (Grobe et al., 2016; Table 1). The maximum temperatures increase with stratigraphic age and are similar on the northern and southern flanks of the Jebel Akhdar Dome (e.g. Natih Fm.). Nahr Umr and Shu’aiba Fm. show slightly higher peak temperatures in the north of the transect (Figure 3). Temperature estimates based on RSCM and solid bitumen reflectance (Grobe et al., 2016) yielded similar temperatures for the southern flank of 248-280 °C for the Nahr Umr, 226-239 °C for the Natih B and 172-206 °C for the Muti, respectively (Table 1, Figure 3). Vitrinite reflectance data of Mozafari et al. (2015) shows temperatures of c. 145-182 °C for Natih B in the Jebel Qusaybah, Adam Foothills, an area not overthrust by the ophiolite complex.

sample No.		location			No. of measurements	mean D_STA	calculated VR_r [%]	mean Temp.
15_995	northern flank	Wadi Yiqah	Sahtan Gp.	M	14	113 +/- 14	6,52	286 +/- 6 °C
15_997		Wadi Yiqah	Shu'aiba	M	10	115 +/- 5	6,69	289 +/- 3 °C
15_1001		Wadi Taisa	Kh 2	M	1	78	8,19	305 °C
15_1003		Wadi Taisa	Kh 2	M	8	96 +/- 9	7,44	297 +/- 4 °C
15_1008		Wadi Taisa	top of Kh 2	M	8	113 +/- 15	6,78	290 +/- 7 °C
15_1010		Wadi Taisa	Shu'aiba	M	13	98 +/- 11	7,28	295 +/- 5 °C
15_1010		Wadi Taisa	Shu'aiba	P	4	149 +/- 15	5,31	270 +/- 9 °C
16_974		Tr- Jur fault	base Sahtan Gp.	P	6	125 +/- 17	6,29	283 +/- 9 °C
16_977		Kharb Plateau	base Natih Fm.	M	10	156 +/- 9	5,04	266 +/- 6 °C
16_979		Kharb Plateau	top Nahr Umr Fm.	M	2	117 +/- 4	6,60	288 +/- 2 °C
16_981		Kharb Plateau	top Nahr Umr Fm.	M	1	149	5,30	270 °C
16_984		Wadi Taisa	Kh 2	M	3	172 +/- 26	5,29	268 +/- 22 °C
16_985		Wadi Murri	Shu'aiba	M	2	90 +/- 4	7,69	300 +/- 2 °C
Grobe et al. (2016)_SV10	southern flank	Wadi Nakhr	Natih	P	6	-	2,83	227-231 °C
Grobe et al. (2016)_AG22		Wadi Nakhr	Natih	M	4	-	3,72	225-260 °C
Grobe et al. (2016)_AG01		Wadi Nakhr	Shu'aiba (Kh 3)	M	4	-	4,49	251-269 °C
Grobe et al. (2016)_AG11		Sint	Hawasina	P	5	-	2,45	193-213 °C
Grobe et al. (2016)_AG25		Balcony Walk Nakhr	Nahr Umr	M	4	-	4,23	226-267 °C
Grobe et al. (2016)_AG26_1		Balcony Walk Nakhr	Nahr Umr	P	2	-	(2.58)	(211-213 °C)
Grobe et al. (2016)_AG26_3		Balcony Walk Nakhr	Nahr Umr	M	2	-	4,96	275-280 °C
Grobe et al. (2016)_AG27		Balcony Walk Nakhr	Nahr Umr	M	3	-	4,61	248-266 °C
Grobe et al. (2016)_AG30		Balcony Walk Nakhr	Nahr Umr	M	3	-	4,25	248-257 °C
Grobe et al. (2016)_AG37		Jebel Shams	Muti	P	3	-	2,16	191-208 °C
Grobe et al. (2016)_AG38		Jebel Shams	Muti	P	2	-	1,99	172-206 °C
reference		**location**			**No. of measured particles**	**measured BR_r [%]**	**calculated / measured VR_r [%]**	**calculated T_{burial} (Barker and Pawlewicz, 1994)**
Grobe et al. (2016)	N south. fl.	Wadi Nakhr area	Natih B	BR_r	253	3.08-3.59	3.08-3.59	226-239 °C
Fink et al. (2015)		Wadi Nakhr area	Natih B	BR_r	200	3.10-3.14	-	c. 225 °C
Fink et al. (2015)		Wadi Nakhr area	Natih A Vein	BR_r	c. 250	3.40-3.76	-	-
Grobe et al. (2016)		Al Hamra area	Natih B	BR_r	20	2.95-3.34	2.95-3.34	223-233 °C
Grobe et al. (2016)		Wadi Sahtan	Natih B	BR_r	6	3,32	3,32	232 °C
Mozafari et al. (2015), measured at RWTH		Jebel Qusaybah	Natih B	VR_r	25		1,8	c. 182 °C
		Jebel Qusaybah	Natih B	VR_r	20		1,1	c. 145 °C

Table 1: Thermal maturity data and calculated peak temperatures of northern Oman. Temperatures from Raman spectroscopy of carbonaceous material are calculated based on the STA approach of Lünsdorf (2016) and the formula published by Grobe et. al (2016). M/P indicate if measurement was conducted on solid bitumen particles (P) or below the surface of the matrix (M). Data of Mozafari et al. (2015) are used for Jebel Qusaybah, Adam Foothills.

4.2. Thermochronology

Results of the ZHe dating are shown in figures 3Figure 3 and 4; time-temperature paths modeled with HeFTy are included in the electronic supplement (Figures S3 and S4). Samples from the carbonate platform (stratigraphically older than Muti Fm.) have been entirely reset after deposition (Figure 3). This coincides with the center of the Jebel Akhdar Dome in which all cooling ages fall in the range of 48.7 ± 1.8 to 39.8 ± 3.0 Ma (Table 2, Figure 4). Sample T4, collected in the Muti Fm., yields an apparent mean age of 93.8 ± 6.9 Ma and samples T5 and T7 of the Hawasina Nappes collected at the northern and the southern slope of the dome, show two grain age populations of 43.0 ± 3.7 / 99.2 ± 8.5 Ma, and 58.9 ± 7.0 / 106.0 ± 5.2 Ma, respectively. In sample T5, an additional single grain age population of 172.9 ± 14.9 Ma was obtained.

sample	lithology / location		He		^{238}U			^{232}Th			Th/U	Sm			ejection	uncorrected	FT corrected			mean age [Ma]		
aliquot	Easting	Northing	vol. [ncc]	1 σ [%]	mass [ng]	1 σ [%]	conc. [ppm]	mass [ng]	1 σ [%]	conc. [ppm]	ratio	mass [ng]	1 σ [%]	conc. [ppm]	correct. (Ft)	He age [Ma]	He age [Ma]	2σ [%]	2σ [Ma]			
T1-Z1	sandstone		5,31	0,83	1,04	1,81	212,00	0,38	2,41	77,66	0,37	0,03	10,43	6,44	0,754	38,90	**51,60**	8,20	4,20	**48,70**	**+/-**	**1,80**
T1-Z2	547533	2574875	6,05	0,84	1,31	1,81	323,34	0,33	2,41	80,49	0,25	0,01	21,24	2,97	0,737	36,10	**49,10**	8,70	4,30			
T1-Z3	Fara Fm.	Autochthon A	3,45	0,87	0,84	1,81	212,21	0,30	2,41	74,73	0,35	0,02	14,08	3,83	0,719	31,30	**43,60**	9,20	4,00			
T1-Z4			3,15	0,86	0,64	1,82	178,10	0,34	2,41	95,86	0,54	0,01	15,61	4,16	0,72	36,30	**50,50**	9,10	4,60			
T2-Z1	tuffite		9,23	0,83	2,04	1,81	352,85	1,03	2,41	178,16	0,50	0,04	9,53	7,26	0,778	33,40	**42,90**	7,60	3,20	**46,10**	**+/-**	**2,00**
T2-Z2	547533	2574875	8,58	0,83	1,99	1,81	376,54	0,88	2,41	166,07	0,44	0,07	7,63	14,20	0,757	32,30	**42,70**	8,10	3,50			
T2-Z3	Fara Fm.	Autochthon A	12,48	0,83	2,32	1,81	377,81	1,01	2,41	163,95	0,43	0,03	11,07	5,44	0,789	40,20	**51,00**	7,30	3,70			
T2-Z4			6,16	0,83	1,26	1,81	186,92	0,52	2,41	76,65	0,41	0,03	10,98	4,83	0,768	36,80	**48,00**	7,80	3,80			
T3-Z1	sandstone		3,69	0,86	1,04	1,81	361,71	0,41	2,41	142,73	0,39	0,02	15,90	6,29	0,689	26,90	**39,10**	10,00	3,90	**42,60**	**+/-**	**1,70**
T3-Z2	544722	2570255	2,82	0,88	0,63	1,82	254,57	0,22	2,42	87,47	0,34	0,02	12,85	9,07	0,694	34,20	**49,40**	9,90	4,90			
T3-Z3	Muaydin Fm.	Autochthon A	1,54	0,90	0,35	1,85	116,01	0,23	2,42	75,70	0,65	0,02	17,64	5,19	0,67	31,80	**47,50**	10,50	5,00			
T3-Z4			4,71	0,84	1,20	1,81	309,13	0,70	2,41	180,18	0,58	0,05	9,18	12,12	0,74	28,50	**38,50**	8,60	3,30			
T3-Z5			8,91	0,83	1,95	1,81	262,57	1,30	2,41	175,08	0,67	0,07	9,00	9,29	0,761	32,60	**42,90**	8,00	3,40			
T3-Z6			9,80	0,83	2,52	1,81	283,31	1,13	2,41	127,16	0,45	0,06	7,80	6,56	0,816	29,00	**35,60**	6,60	2,30			
T3-Z7			11,83	0,83	2,41	1,81	219,27	1,23	2,41	111,66	0,51	0,11	7,31	10,01	0,794	36,10	**45,50**	7,10	3,20			
T3-Z8			8,41	0,83	1,85	1,81	224,86	1,04	2,41	125,92	0,56	0,07	9,09	8,40	0,784	33,10	**42,20**	7,40	3,10			
T4-Z1	conglomerate		18,23	0,83	1,79	1,81	380,98	0,44	2,41	93,57	0,25	0,02	13,79	3,77	0,736	79,30	**107,60**	8,70	9,40	**93,80**	**+/-**	**6,90**
T4-Z2	517510	2560808	10,68	0,83	1,36	1,81	392,55	0,35	2,41	100,65	0,26	0,02	15,99	5,30	0,703	61,20	**86,90**	9,60	8,40			
T4-Z3	Muti Fm.	Autochthon B	5,24	0,85	0,56	1,82	137,78	0,48	2,41	118,23	0,86	0,04	8,48	11,06	0,738	64,20	**86,90**	8,60	7,50			
T5-Z1	turbiditic sandstone		34,15	0,82	3,38	1,81	502,17	0,79	2,41	117,95	0,23	0,10	7,97	14,16	0,781	78,70	**100,80**	7,50	7,60	**106,00**	**+/-**	**5,20**
T5-Z2	512934	2561691	13,52	0,83	1,28	1,81	333,42	0,27	2,41	69,42	0,21	0,02	16,57	4,11	0,744	82,70	**111,20**	8,50	9,50			
T5-Z3	Matbat Fm.	Hawasina N.	8,95	0,83	1,30	1,81	254,43	0,78	2,41	153,35	0,60	0,01	16,47	2,78	0,754	49,70	**65,90**	8,20	5,40	**58,90**	**+/-**	**7,00**
T5-Z4			9,21	0,84	1,75	1,81	416,93	0,69	2,41	163,29	0,39	0,04	9,44	9,25	0,766	39,80	**51,90**	7,90	4,10			
T5-Z5			37,88	0,80	51,13	2,33	1,81	561,72	0,37	2,41	90,14	0,16	0,02	11,59	0,741	128,10	**172,90**	8,60	14,90			
T6-Z1	granodiorite		6,55	0,83	1,00	1,81	241,80	1,28	2,41	311,91	1,29	0,29	5,62	69,36	0,747	41,60	**55,60**	8,30	4,60	**53,70**	**+/-**	**1,20**
T6-Z2	478301	2592360	6,39	0,85	0,97	1,81	288,96	1,32	2,41	394,16	1,36	0,28	5,31	84,38	0,719	41,10	**57,20**	9,10	5,20			
T6-Z3	Trondjemite	Semail Ophio.	7,07	0,83	1,06	1,81	314,75	1,79	2,41	528,55	1,68	0,19	5,49	57,19	0,751	39,20	**52,30**	8,20	4,30			
T6-Z4			12,11	0,84	1,79	1,81	347,26	3,35	2,41	649,55	1,87	0,31	5,55	61,00	0,769	38,60	**50,20**	7,70	3,80			
T6-Z5			6,78	0,84	1,08	1,81	273,36	1,46	2,41	368,85	1,35	0,27	5,75	68,70	0,738	39,10	**53,00**	8,60	4,50			
T7-Z1	quarzite		14,91	0,84	1,56	1,81	427,30	0,43	2,41	118,20	0,28	0,05	9,26	12,45	0,744	73,80	**99,20**	8,50	8,50	**99,20**		
T7-Z2	514817	2586049	4,14	0,87	1,35	1,81	428,75	0,38	2,41	119,50	0,28	0,02	12,47	7,90	0,729	23,70	**32,50**	8,90	2,90	**43,00**	**+/-**	**3,70**
T7-Z3	Matbat Fm.	Hawasina N.	6,37	0,85	1,33	1,81	274,36	0,30	2,41	62,67	0,23	0,03	10,62	6,71	0,769	37,50	**48,80**	7,90	3,80			
T7-Z4			9,66	0,81	12,43	2,13	1,81	539,06	0,15	2,45	38,38	0,07	0,01	17,24	0,777	36,90	**47,50**	7,70	3,70			
T7-Z5			4,03	0,83	5,46	0,94	1,81	232,12	0,47	2,41	115,05	0,50	0,02	12,63	0,738	31,70	**43,00**	8,60	3,70			
T8-Z1	tuffitic sandstone		4,60	0,86	1,34	1,81	450,89	1,11	2,41	374,66	0,83	0,16	5,81	53,52	0,759	23,70	**31,20**	8,00	2,50	**39,80**	**+/-**	**3,00**
T8-Z2	532600	2578681	2,92	0,85	0,56	1,82	147,09	0,86	2,41	226,75	1,54	0,28	5,14	73,06	0,715	31,40	**44,00**	9,20	4,00			
T8-Z3	Mistal Fm.	Autochthon A	2,21	0,89	0,46	1,83	168,48	0,57	2,41	208,48	1,24	0,05	8,65	16,66	0,716	30,90	**43,20**	9,20	4,00			
T8-Z4			3,46	0,85	0,85	1,81	212,57	0,41	2,41	103,10	0,49	0,01	14,27	3,65	0,74	30,30	**41,00**	8,60	3,50			
T9-Z1	quarzite		2,90	0,86	0,61	1,82	238,35	0,50	2,41	198,12	0,83	0,01	16,09	5,23	0,705	33,10	**46,90**	9,50	4,50	**45,50**	**+/-**	**2,40**
T9-Z2	532595	2568258	0,72	0,98	0,18	1,94	109,52	0,13	2,43	76,58	0,70	0,05	10,52	29,38	0,674	27,50	**40,80**	10,50	4,30			
T9-Z3	Mistal Fm.	Autochthon A	2,04	0,89	0,41	1,84	147,39	0,28	2,41	101,51	0,69	0,01	18,70	3,60	0,718	35,10	**48,80**	9,20	4,50			
T10-Z1	sandstone		5,09	0,85	0,93	1,81	213,39	0,95	2,41	217,83	1,02	0,02	13,41	4,93	0,754	36,40	**48,20**	8,10	3,90	**46,90**	**+/-**	**4,10**
T10-Z2	534779	2572636	6,71	0,83	1,37	1,81	267,61	1,24	2,41	241,07	0,90	0,04	9,18	8,32	0,763	33,30	**43,70**	7,90	3,40			
T10-Z3	Mistal Fm.	Autochthon A	8,97	0,83	2,25	1,81	568,33	1,79	2,41	452,52	0,80	0,04	8,74	10,22	0,723	27,70	**38,40**	9,00	3,50			
T10-Z4			2,26	0,88	0,35	1,85	118,10	0,39	2,41	131,18	1,11	0,02	14,08	5,39	0,727	41,80	**57,50**	8,90	5,10			
T11-Z1	quarzite		4,70	0,84	1,01	1,81	188,02	0,57	2,41	106,02	0,56	0,01	19,39	2,18	0,746	34,00	**45,60**	8,40	3,80	**42,50**	**+/-**	**2,00**
T11-Z2	540394	2572230	1,55	0,90	0,39	1,84	109,55	0,33	2,41	93,99	0,86	0,01	20,85	2,31	0,706	27,30	**38,80**	17,60	6,80			
T11-Z3	Mistal Fm.	Autochthon A	1,50	0,94	0,37	1,84	110,19	0,19	2,42	56,69	0,51	0,01	17,25	3,39	0,693	29,90	**43,20**	9,90	4,30			
T12-Z1	sandstone		5,35	0,85	1,21	1,81	355,93	1,09	2,41	320,43	0,90	0,02	16,47	5,58	0,706	30,10	**42,70**	9,50	4,00	**40,10**	**+/-**	**1,50**
T12-Z2	531776	2582871	4,28	0,86	1,12	1,81	286,68	0,16	2,42	40,59	0,14	0,01	27,93	1,79	0,736	30,70	**41,70**	8,80	3,70			
T12-Z3	Sahtan Gp.	Autochthon B	3,80	0,86	1,06	1,81	349,54	0,14	2,43	44,41	0,13	0,01	22,03	2,70	0,719	28,70	**39,90**	9,20	3,70			
T12-Z4			1,51	0,89	0,38	1,84	92,50	0,32	2,41	76,60	0,83	0,01	15,61	3,53	0,758	27,30	**36,10**	8,10	2,90			

Table 2: Results of zircon (U-Th)/He dating.

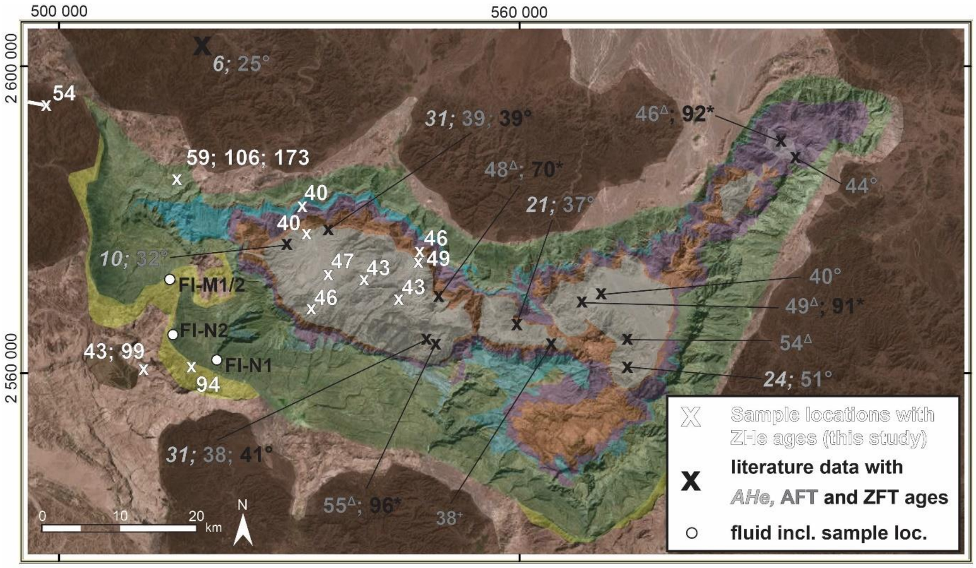

Figure 4: Map view of ZHe ages sampled below, in and above the carbonate platform of the Jebel Akhdar Dome. Data outlines a general cooling between 58.9 ± 7.0 and 39.8 ± 3.0 Ma. Some samples outside of the dome show two age populations, with an additional age population of c. 100 Ma. Additional temperature data refers to zircon fission track ages of (*) Saddiqi et al. (2006), Apatite fission track ages of (Δ) Poupeau et al. (1998) and (+) Mount et al. (1998), and AHe, AFT and ZFT ages of (+, grey) Hansmann et al. (2017). Moreover, the locations of samples used for fluid inclusion measurements are shown. Colors in the background depict geological units as defined in Figure 4.

These ages indicate a large-scale cooling signal that affects the entire study area and is associated with doming. The ZHe age pattern and 1D thermal models (Figures S3 and S4) indicate a phase of rapid cooling below 170 °C in the early Cenozoic (58.9 ± 7.0 and 39.8 ± 3.0 Ma). The range of modeled cooling paths outline minimum and maximum cooling rates of 2-8 °C/Myr. This is followed by slower cooling until the present day.

Data from the Muti Fm. and the Hawasina units differ partly from this trend: the apparent ZHe age of the Muti sample T4 (93.8 ± 6.9 Ma) is as old as its respective stratigraphic age (Turonian-Campanian; Robertson, 1987) indicating only partial reset of the ZHe system. Samples of the lower Hawasina Nappes contain two grain age populations. Older ages coincide with higher uranium concentrations suggesting that only the younger ages represent thermally reset zircons. The older ZHe population of 110-95 Ma coincides with timing of forebulge migration through the area, as independently determined in the stratigraphic record in the Wasia-Aruma Break (Figure 3). Partial reset of ZHe ages suggests that the Hawasina samples have not experienced temperatures exceeding the partial retention zone (PRZ) of 150-170 °C.

A magmatic sample of an intrusive from the Semail Ophiolite yields ZHe ages of 53.7 ± 1.2 Ma (T6) with a modeled cooling path gradually decreasing into the PRZ until c. 55 Ma. This time interval of passing the PRZ is comparable to the Hawasina nappe samples beneath the ophiolite but occurs slightly earlier than cooling of the Autochthonous. Nevertheless, Semail Ophiolite, Hawasina Nappes and the autochthonous margin sequence were affected by the same cooling event that was possibly initiated by exhumation of the Jebel Akhdar Dome.

4.3. Fluid inclusions

The Muti veins' samples FI-M1 and M2 of the southern Jebel Akhdar show evidence of crack and seal processes (youngest parts in the center of the vein, Ma-2010-11b and 14a of Arndt 2015) with blocky quartz grains that contain two kinds of roundish primary FIs with sizes of 3-20 µm. They are mainly aligned along dark zones and are interpreted as growth zones or form bright clusters in the central part of the crystals. A third set of fluid inclusions (FIs) appears in large, grain-crosscutting trails interpreted to be of secondary origin. Calcite crystals within the Natih veins contain bright FIs with sizes of 2-20 µm and are edgy, often rectangular or trapezoidal in shape. Identified primary FIs are aligned parallel to crystal growth zones.

All measured FIs are two-phase, liquid-vapor inclusions with ice as last phase to melt. The Muti samples show $T_{fm(ice)}$ between -5.1 ± 0.5 and -4.6 ± 0.3 °C and $T_{m(ice)}$ at -2.2 ± 0.2 to -1.9 ± 0.1 °C, the Natih sample T_{fm} of -18.4 ± 1.9 to -20.2 ± 2.1 °C and $T_{m(ice)}$ of -7.1 ± 0.3 to -8.9 ± 1.8 °C (Table 3). First melting temperatures of all inclusions correspond to an H_2O-NaCl system and complete melting temperatures of ice indicate salinities similar to seawater (3.0 ± 0.5 to 3.5 ± 0.3 wt.-% NaCl eq., Muti Fm.) or three times higher (10.3 ± 0.3 to 12.5 ± 2.0 wt.-% NaCl eq., Natih Fm.).

Table 3: Results of FI thermometry. Identified FI types, their measured homogenization temperatures and results of the pressure correction for 280 and 340 MPa accounting for 8 and 10 km of ophiolite with partly serpentinized mantle sequence and 2 km of sedimentary nappes, and for 45 MPa accounting for 2 km of sedimentary overburden for samples unaffected by ophiolite obduction. First melting (T_{fm}) and final melting of ice ($T_{m\ ice}$) temperatures and salinities are given. Data of Holland et al. (2009) is added for comparison and we likewise corrected his homogenization temperatures for pressures of 280 and 340 MPa, as his samples were originally covered by the ophiolite complex. (* further heating was avoided to prevent inclusion damage)

sample No.	vein orient., location and host mineral	FI kind	No. of FIA	T_{hom} [°C]	pressure corrected T [°C] for 45 MPa		T_{fm} [°C]	$T_{m\ ice}$ [°C]	salinity [wt.-% NaCl]
FI-M1	**NE-SW striking**	primary	21	166 +/- 7	189 +/- 7		-4.7 +/- 0.2	-2.2 +/- 0.2	3.5 +/- 0.3
	strike-slip vein (IX), Muti Fm.	primary	22	189 +/- 3	213 +/- 3		-4.6 +/- 0.3	-2.0 +/- 0.3	3.2 +/- 0.4
	Gorge area, quartz	secondary	18	> 200*	> 224		-4.6 +/- 0.2	-2.0 +/- 0	3.2 +/- 0
					pressure corrected T [°C] for 45 MPa				
FI-M2	**NE-SW striking**	primary	24	161 +/- 3	184 +/- 3		-5.1 +/- 0.5	-1.9 +/- 0.1	3.0 +/- 0.2
	strike-slip vein (IX), Muti Fm.	secondary	12	116 +/- 12	138 +/- 12		-	-	-
	Gorge area, quartz	secondary	24	150 +/- 2	172 +/- 2		-	-	-
					for 280 MPa	**for 340 MPa**			
FI-N1	**Natih Fm., NW-SE**	primary	14	90 +/- 5	235 +/- 5	266 +/- 5	-18.4 +/- 1.9	-7.1 +/- 0.3	10.3 +/- 0.3
	burial vein (III), Wadi Nakhr, calcite	primary	26	(114 +/- 7)	(264 +/- 7)	(297 +/- 7)	-20.2 +/- 2.1	-8.9 +/- 1.8	12.5 +/- 2.0
FI-N2	**Natih Fm., early E-W vein (I)** **Al Raheba, calcite**	primary	10	80 +/- 4	225 +/- 4	256 +/- 4	-	-	-
					for 280 MPa	**for 340 MPa**			
Holland et al. (2009)	**Sahtan Gp., bedding parallel shear vein, top-to-NE (IV), Wadi Nakhr, quartz**	primary and pseudosec.	n.a.	134-141	296-303	357-364	from -19	-3.7 to -2.3	3.8 to 6.0

Primary inclusions in quartz crystals from the Muti Fm. show minimum trapping temperatures of 161 ± 3 to 166 ± 7 °C (Table 3, FI-M2 and middle of FI-M1) with a second primary population of 189 ± 3 °C (sides of vein FI-M1). T_h of secondary inclusions in FI-M1 are above 200 °C. In sample FI-M2, two generations of secondary inclusions were observed, both reflecting lower T_h than the primary inclusions. No hints of necking down, leakage or stretching were observed at the measured inclusions and over 90 % of the measured FIs in one assemblage are in the range of 10-15 °C representing a good quality of the measurements (Goldstein, 2001).

Samples FI-N1 and N2 of the Natih Fm. in the southern Jebel Akhdar (Figure 4) contain primary inclusions hosted by calcite crystals giving T_h of 80 ± 4, 90 ± 5 and 114 ± 7 °C (Table 3). The latter population is often characterized by elongated, possibly stretched FI, and is not considered for further interpretations. Assuming vein formation during burial (Grobe et al., 2018; Hilgers et al., 2006; Holland et al., 2009; Virgo, 2015) under 8 to 10 km of ophiolite including partially serpentinized peridotite and 2 km of Hawasina Nappes, results were pressure corrected for 280 and 340 MPa leading to corrected homogenization temperatures of 235 ± 5 and 266 ± 5 °C (FI-N1), and 225 ± 4 and 256 ± 4 °C (FI-N2, Table 3). Signs of strong deformation such as twinning or cleavage were not observed in the measured inclusions; secondary inclusions were present but not measured.

These temperatures represent minimum trapping conditions of a paleo-fluid and do not necessarily represent burial temperatures of the host rock. It should be noted that the analyzed Natih veins formed bedding confined (Grobe et al., 2018; Holland et al., 2009; Virgo, 2015) and show host rock buffered carbonate isotope signatures (Arndt et al., 2014; Hilgers et al., 2006). This corroborates the idea that analyzed veins were in thermal equilibrium with their host rocks.

FI thermometry of late strike-slip veins in the Muti Fm. are interpreted to have formed after dome formation (Grobe et al., 2018; Virgo, 2015) at an assumed depth of 2 km. A pressure correction for the related 45 MPa corresponds to minimum fluid trapping temperatures of 184 ± 3 °C (FI-M2) and 213 ± 3 °C (FI-M1) with a later phase of primary inclusions outlining 189 ± 7 °C and even cooler secondary inclusions of 138 ± 12 to 172 ± 2 °C (FI-M1 and M2, Table 3). These cooler fluid temperatures can be explained by further exhumation of the Jebel Akhdar and, hence, cooling of the fluids' reservoir during crack-seal vein formation. Isotope studies on the vein calcite do not support an open system with fluid exchange (Stenhouse, 2014; Virgo and Arndt, 2010), hence, we interpret the formation of strike-slip related veins as having formed during exhumation following peak burial.

Based on the assumption that fluid and host rock were in thermal equilibrium, we can use maturity data in combination with fluid inclusion data to estimate the pressure at vein formation. Peak temperatures of the Sahtan Fm. revealed by RSCM reached 283 ± 9 to 286 ± 6 °C (Table 1, Figure 5 red line) and enable to solve the pressure-temperature couples of FIs measured in Sahtan veins formed at deepest burial by Holland et al. (2009, black line). This results in minimum trapping pressures of 254 ± 30 MPa at times of vein formation (Figure 5 blue line), which correspond to times close to or at deepest burial of the carbonate platform.

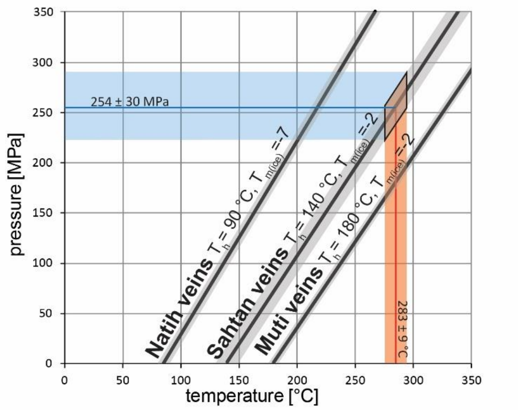

Figure 5: Fluid inclusion isochores (solid black lines) of analyzed fluid inclusion populations with corresponding std. deviations (shaded areas, for Sahtan Gp. data of Holland et al., 2009, conservatively ± 10°C are assumed). To estimate the pressure conditions during vein formation, calculated temperatures from thermal maturity data are added for the Sahtan Gp. (red line with error) and result in minimum trapping pressures of 254 ± 30 MPa during peak burial (blue line with error).

4.4. Structural observations

The reconstructed transect (Figure 2) shows the dome structure of the Jebel Akhdar covered with ophiolite nappe remnants in the northeast, the thrusted southern foreland and the salt basins in the southeast that contain the fault-bound hydrocarbon reservoirs of the Fahud and Natih fields. Structures shown are related to large scale normal faulting in the mountain area, where faults are subsequently rotated and bent by doming (Jebel Akhdar), and later strike-slip faulting crosscut domed layers (Gomez-Rivas et al., 2014; Grobe et al., 2018; Virgo, 2015). Reactivation and inversion of some of the strike-slip faults caused formation of hydrocarbon traps in the southern foreland (Natih and Fahud field, e.g. Al-Kindi and Richard, 2014).

4.5. Basin modeling

Numerical basin modeling integrates all data and tests the individual interpretations in the thermal and geodynamic framework. Deepest burial was constrained with thermal maturity data and exhumation with thermochronological data. In the following we present our best fit model, considering a mixed ophiolite lithology (Searle and Cox, 2002) consisting of strongly serpentinized peridotites. Then, the sensitivity of important results to changes of relevant input parameters are discussed.

Modeled evolution of the transect over time is given in Figures 8 and 9, showing (a) final deposition of the Autochthonous B, (b) erosion of the Natih Fm. in the North by a moving foredeep, (c) emplacement of Hawasina Nappes, and d-e) ophiolite obduction reconstructed by rapid, stepwise sedimentation. After maximum burial beneath the ophiolite complex at c. 80 Ma (Warren et al., 2005) exhumation is assumed to start slightly prior to 55 Ma (Saddiqi et al., 2006) with a rapid phase of cooling below c. 200 °C at 55 Ma leading to lower temperatures in the Jebel Akhdar region. 1D burial plots of two pseudo-wells created out of point data in Wadi Nakhr and Wadi Yiqah are shown in the electronic supplement Figure S5.

Solid Earth Discuss., https://doi.org/10.5194/se-2018-78
Manuscript under review for journal Solid Earth
Discussion started: 14 August 2018

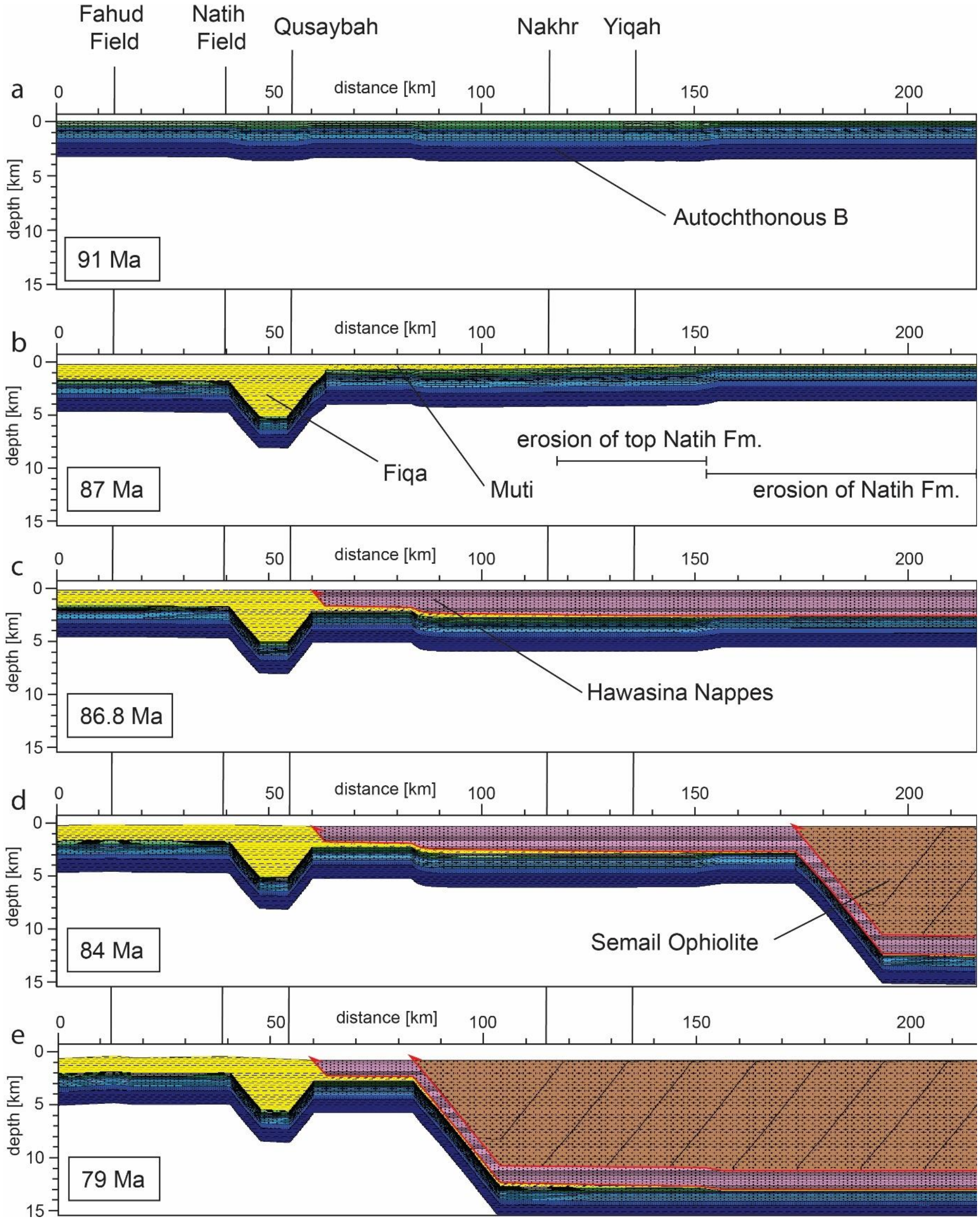

Figure 6: Modeling results: Transect evolution from sedimentation of the Autochthonous B at stable passive margin conditions (a), to moving foredeep that finally filled with Fiqa sediments (b, peak burial as calibrated by thermal maturity data), Hawasina Nappe (c) and ophiolite emplacement (d) leading to deepest burial (e). Highlighted with vertical lines in the background are the locations of present-day oil fields and sampling sites.

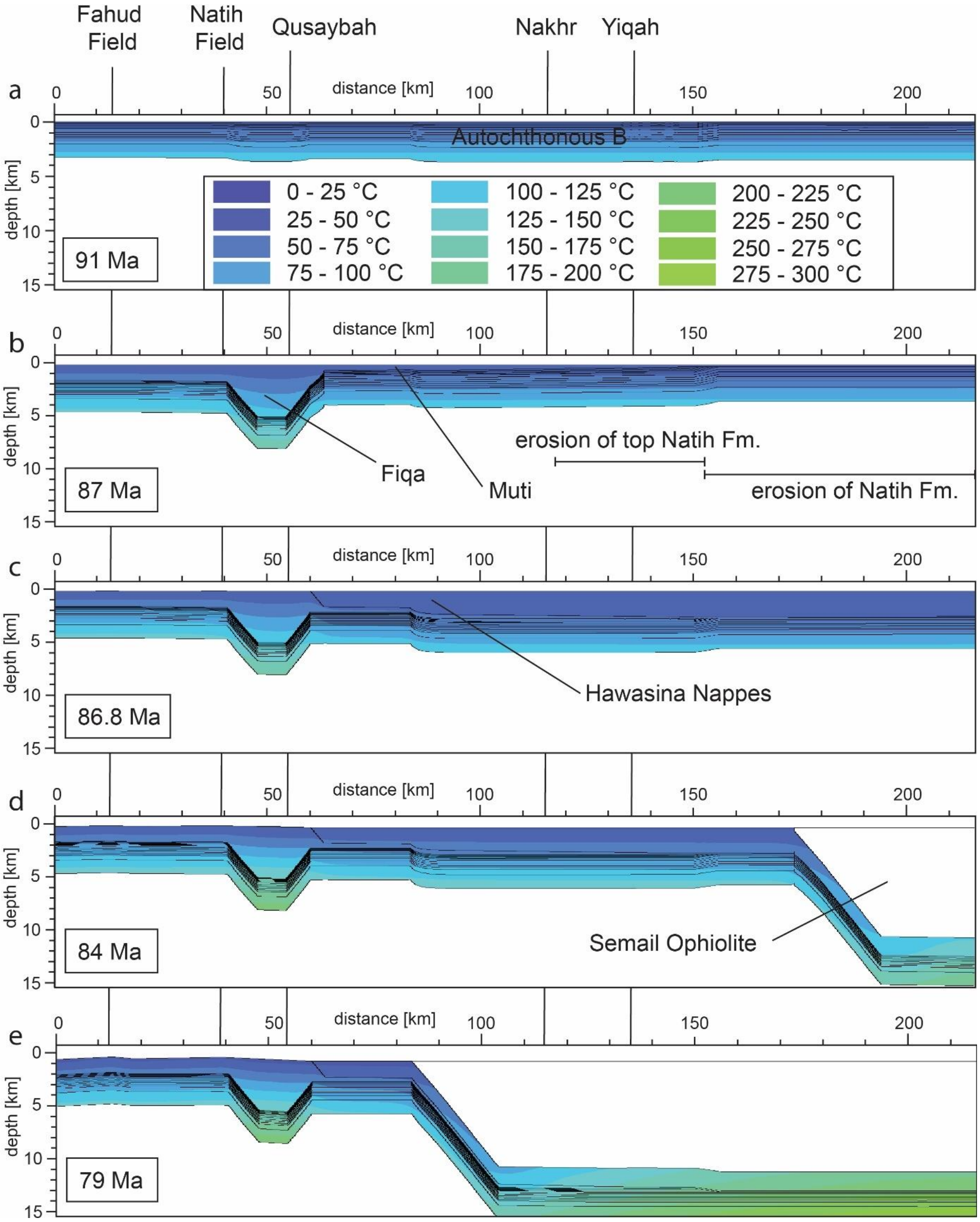

Figure 7: Modeling results: Temperature evolution of the transect of Figure 6. Highlighted with vertical lines in the background are the locations of present-day oil fields and sampling sites.

As a model set up only presents one possible solution out of several, sensitivity analyses with varying paleo-overburden thicknesses (Figures 8 and 9), changing degree of serpentinization of the ophiolite and varying basal heat flow during deepest burial (Figure 10) are presented and discussed below.

Thermal maturity data of the Natih B at Jebel Qusaybah (1.1-1.8 % VR_r), Adam Foothills, requires peak temperatures of 145-182 °C (Table 1). Sensitivity analyzes of the overburden above the Natih Fm. outlined that at least 4 to 4.5 km of sedimentary overburden (Figures 8a and 9a) are needed to match the calibration data.

a) Temperature evolution: Foredeep / Jebel Qusaybah

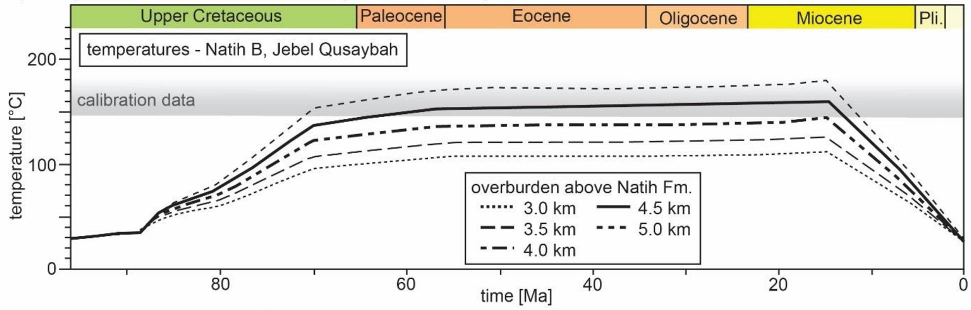

b) Temperature evolution: S-Flank / Wadi Nakhr

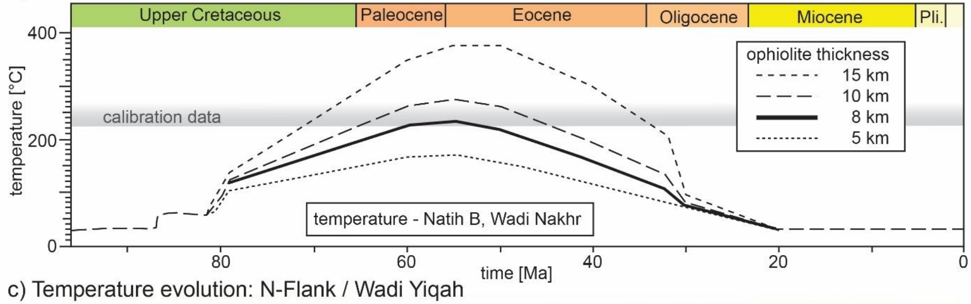

c) Temperature evolution: N-Flank / Wadi Yiqah

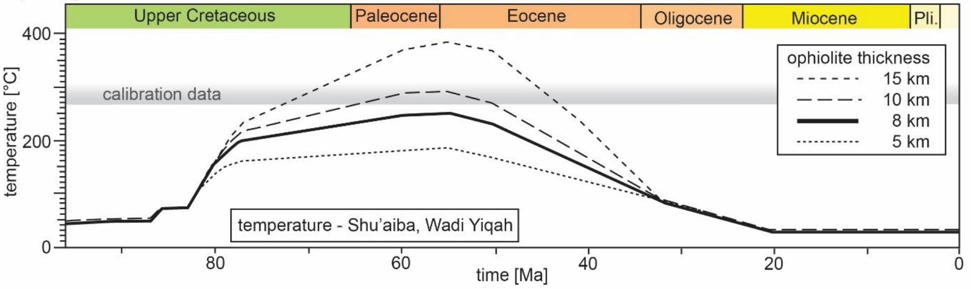

Figure 8: Sensitivity analysis of paleo-overburden and its influences on temperature in comparison to calculated peak temperatures (gray area) for pseudo-wells at Jebel Qusaybah (a), Wadi Nakhr (b) and Wadi Yiqah (c).

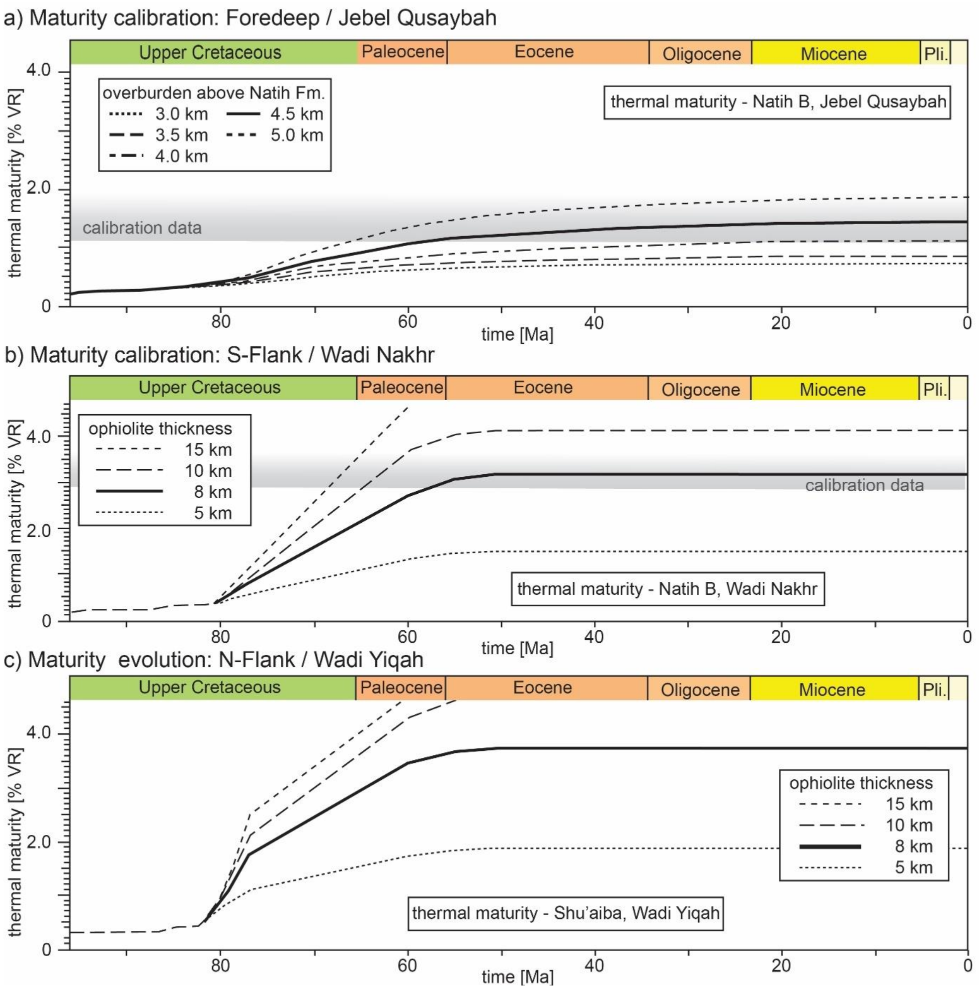

Figure 9: Sensitivity analysis of paleo-overburden and its influences on thermal maturity in comparison to calibration data (gray area). Data is used to calibrate burial depth of the foredeep at the Jebel Qusaybah (a), paleo-ophiolite thickness at the southern flank of the Mountains at Nakhr (b) and at its northern counterpart at Yiqah (c).

To restore the former thickness of the Semail Ophiolite the thickness of the Hawasina Nappes along the transect was fixed to 2 km, representing its minimum thickness as suggested by the maximum present-day thickness of the Jebel Misht exotics. To reach required thermal conditions measured at the entrance of the Wadi Nakhr (Natih B: 2.83-3.72 % VR_r, 225-260 °C; Grobe et al. 2016), 8-10 km of original, total thickness of strongly serpentinized ophiolite sequence are needed in addition to the assumed 2 km of Hawasina Nappes (Figures 8b and 9b). These thicknesses are also sufficient to reach peak temperatures calculated for older stratigraphy at the northern flank of the Jebel Akhdar Dome (Shu'aiba Fm. at Wadi Yiqah: 270-295 °C by RSCM, Figures 8c and 9c). Modeling results show a longer-lasting, quicker increase in maturity and temperature in the north, which we interpret as associated with the 2 Mys earlier onset of obduction and, hence, a longer burial of the northern carbonate platform (Wadi Yiqah) under the active ophiolite obduction compared to is southern counterpart (Wadi Nakhr; Béchennec et al., 1990; Cowan et al., 2014).

Another factor influencing the modeling results is related to the lithology of the overburden and its compaction. In the special case of burial under an ophiolite, serpentinization of peridotite and its impact on ophiolite density and thermal conductivity must be considered. Sensitivity analysis of ophiolite serpentinization shows the temperature and thermal maturity effects on our model (Figure 10). A model-case of ophiolite without any serpentinized peridotite (0 %-case, ρ_{ophio}=3133 kg/m^3) would represent the largest deviation compared to our best-case model assuming complete ophiolite serpentinization (100 %-case, ρ_{ophio}=3069 kg/m^3). This density is based on Al-Lazki et al. (2002). Even if the upper part of the ophiolite is missing in the Jebel Akhdar area, this and the observations of Searle and Cox (2002) in the Saih Hatat support strong serpentinization. A less serpentinized ophiolite means higher densities and related higher thermal conductivities of the overburden and thus lower peak temperatures in the sediments below. In a no-serpentinization case, peak temperature of Natih B in the Wadi Nakhr would decrease by c. 60 °C resulting in a maximum thermal maturity decrease of 1.5 % VR. The best fit model with an ophiolite thickness of 8-10 km would need additional 3 km of overburden at 0 % serpentinization to equally match the measured thermal maturities. Additional thicknesses of 0.75 km (75 % serpentinization), 1.5 km (50 % serpentinization) and 2.25 km (25 % serpentinization) apply for lower degrees of serpentinization, respectively.

Results depend strongly on basal heat flow (Figure S2). The best fit model of 40 mW/m^2 at deepst burial is typical for a passive continental margin setting. If this heat flow at peak burial would be lowered to 30 mW/m^2 an additional amount of 1.2 km of ophiolitic overburden would be required to achieve a match with thermal calibration data (Figure 10). Increased heat flow values to 50, 60 or 70 mW/m^2 would result in less overburden of -1.3, -2.4 and -3.5 km, respectively (Figure 10).

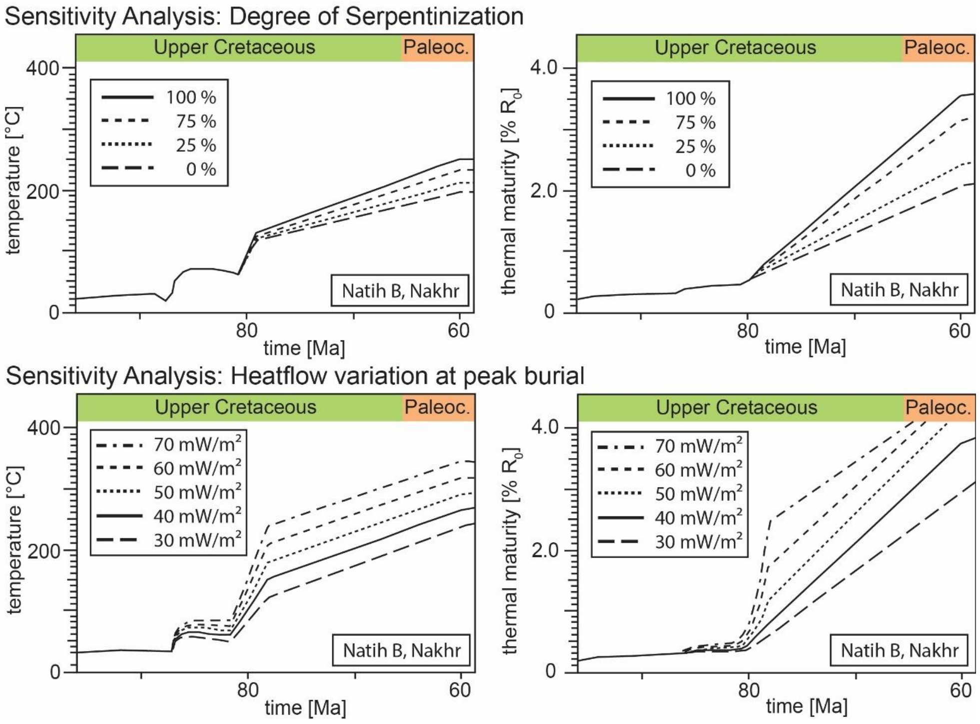

Figure 10: Sensitivity analysis: Top: Different degrees of serpentinization of the peridotite within the Semail Ophiolite affect the temperature (left) and thermal maturity (right) evolution (modeled for Natih B Fm. at Wadi Nakhr). Pure peridotite (0 % serpentinization) require additional 3 km of ophiolite in addition to the 8-10 km of the best-fit model to equally match the calibration data. 100 % refers to complete serpentinization of the peridotite in the ophiolite. Bottom: The influence of variable heat flow values at peak burial on temperature (left) and thermal maturity (right).

5. Discussion

Any basin and petroleum system model has to deal with uncertainties, in particular for complex areas such as the Jebel Akhdar, where sedimentary rocks reached high temperatures and maturities due to deep and rapid burial. In the following, we discuss these uncertainties with respect to temperature and burial history, overpressure build-up and induced fluid flow. For all presented basin models of the study area, the following limitations apply: (1) decompacting the present-day lithologies does not consider rock volume lost by pressure solution. This is probably of minor importance in our study area as host-rock buffered isotope ratios of the veins were interpreted as local sinks for nearby dissolved calcite (Arndt et al., 2014; Hilgers et al., 2006), so that the overall rock volume remains approximately constant, (2) decompaction only accounts for burial, whereas a possible tectonic compaction is neglected (Neumaier, 2015) and (3) calculated overpressure does not include a rock volume decrease due to pressure solution.

5.1. Burial history

Little is known about the very early phase of burial, before 91 Ma (Figures 6 and 7, Grobe et al., 2018). The assumptions for this period are based on hypotheses on the tectonic evolution of the passive continental margin as well as data on thickness of sedimentary units but are not strongly constrained by petrographic data.

In Turonian times (93.9-89.6 Ma; Robertson, 1987) a southwest-ward-moving forebulge, related to plate convergence, affected northern Oman. It eroded the northeastern platform edge and migrated southwest-ward to the present-day position of the Adam Foothills (Robertson, 1987). Measured thermal maturities of 1.1-1.8 % VR_r were used to reconstruct peak temperatures during burial in Jebel Qusaybah, Adam Foothills, which range between 145 and 182 °C. Numerical basin modeling results reveal that additional paleo-overburden of at least 4 to 4.5 km (Natih B, Qusaybah,

Figure 9) is required to reach these temperatures. The exhumation history of the Adam Foothills is not well known; our model is based on an interpreted late exhumation during the Miocene (Claringbould et al., 2013). Earlier exhumation would shorten the time span of the rock at higher temperatures (Figure 7), lead to decreased thermal maturity and, hence, would require additional overburden to match the measured thermal maturity data. Therefore, the resulting burial of 4 to 4.5 km has to be regarded as minimum value, which would increase by pre-Miocene exhumation of the Jebel Qusaybah. South of the Adam Foothills basin geometries are not affected by the moving foredeep. Here peak burial was reached under c. 3 km of Fiqa, Hadhramaut and Fars formations. This is based on the assumption that present-day burial equals deepest burial as no thermal calibration data of the area south of Jebel Qusaybah was achieved, which is in agreement with interpretations of Terken (1999) and Warburton et al. (1990).

In case of the Jebel Akhdar, peak temperatures were reached as a consequence of burial below the ophiolite (e.g. Loosveld et al., 1996; Searle, 2007; Searle et al., 2003; Warren et al., 2005). Here the sedimentary rocks reached high temperatures and maturities as shown by solid bitumen reflectance, RSCM, FT-IR and Rock-Eval pyrolysis data (Table 1; Fink et al., 2015; Grobe et al., 2016). Pre-obduction burial by sedimentation is not sufficient for such high thermal maturities, and it likewise cannot be explained by increased basal heat flow before 91 Ma or after 55 Ma. Influence of local hydrothermal effects cannot be excluded, but because the entire Jebel Akhdar reached high temperatures, short-term, local events are unlikely to have been dominant. A regional thermal overprint on the passive margin sediments by warm ophiolite obduction can be excluded as the peak temperatures in the Jebel Akhdar Dome are increasing with stratigraphic age. This is in agreement with models of Lutz et al. (2004) outlining that even in subduction zones the isotherms of the rapidly buried sediments are not adjusting to the surrounding temperatures instantaneously. Moreover, the thermal imprint as observed by the metamorphic sole in northern Oman is only affecting 10's of meters in the sub-thrust Hawasina Nappes (e.g. Searle and Cox, 2002) and not the carbonate platform sediments below. This only minor sub-thrust thermal overprint is also observed in other thrust zones (e.g. Wygrala, 1989).

To reach measured maturity data in the mountain area of the transect a paleo-thickness of the ophiolite in the order of 8-10 km on top of 2 km of Hawasina Nappes is required (Figure 9); this would account for 280 to 320 MPa of lithostatic pressure and is in rough agreement with the pressure reconstructed by combining fluid inclusion data and independently determined thermal rock maturity temperatures (cf. FI results: 254 ± 30 MPa). Depending on lithological effects, such as a less pronounced serpentinization of the ophiolite, this value might increase by up to 3 km (Figure 10). Basal heat flow values at deepest burial are estimated to c. 40 mW/m². This seems realistic as passive margin conditions prevail, and no magmatism or rifting is reported in the area.

Basin modeling indicates that highest temperatures were reached much later than deepest burial under the ophiolite (Figure 7), directly prior to uplift. This difference is interpreted as time the rock needed for thermal equilibration after rapid burial. Deep burial under the ophiolite represents the only time in basin evolution when ductile limestone deformation was possible (Grobe et al., 2018). However, there is uncertainty concerning the exact timing of deepest burial in the Jebel Akhdar (we used 79 Ma according to U-Pb dating of eclogites in the Saih Hatat window; Warren et al., 2005) and the beginning of early uplift (we used 55 Ma, as discussed below).

Our peak temperatures are in principal agreement with temperatures of c. 200 °C suggested for the top of the carbonate platform by Breton et al. (2004), and non-reset zircon fission tracks in the pre-Permian basement indicating peak temperatures up to 280 °C (Saddiqi et al., 2006). Moreover, thermal maturities of the same stratigraphic units show similar values along the transect and around the dome (Grobe et al., 2016). Hence, we assume a similar burial history for the entire Jebel Akhdar. However, a slightly deeper burial of the northern flank can, within the range of error, not be excluded. The temperatures used in our models are in contrast with recent results on mixed illite-smectite layers and clay mineral assemblages from the Jebel Akhdar by Aldega et al. (2017) who argue for peak temperatures of 150-200 °C on the northern flank of the Jebel Akhdar and 120-150 °C on the southern flank. These values are incompatible with our solid bitumen and Raman spectroscopy data, as well as with the overmature Natih B source rock on the southern flank (data presented here and in Grobe et al. 2016). Independent data on temperatures from fluid inclusions confirm the higher temperature range. At present, there is no clear explanation for this discrepancy. However, it has been shown that the vitrinite reflectance system is more sensitive to rapid temperature changes than clay mineralogy (e.g. Hillier et al., 1995; Velde and Lanson, 1993). If burial was short enough, the clay minerals may not have time to recrystallize, possibly due to a lack of potassium, whereas vitrinite reflectance increases. Another possible explanation may be that the dated clay minerals formed during top-to-NNE shearing, and thus do not show peak burial. Indeed it has been shown that deformation associated with this early extension reaches deeply into the passive margin sequence, and includes the Rayda and

Shuaiba Formations (Grobe et al., 2018; Mattern and Scharf, 2018). Furthermore, Aldega et al. (2017) suggest that the thermal evolution during uplift of Grobe et al. (2016) does not account for thermochronological data in pre-Permian basement rocks (Poupeau et al., 1998; Saddiqi et al., 2006), arguing the 1D thermal models indicate temperature in the basement had to be lower than 70°C during the Eocene-Oligocene. In fact, the raw data from the basement indicate rapid cooling at 55 ± 5 Ma, in agreement with models of Grobe et al. (2016) and the exhumation presented in this work.

Temperatures of the ductile top-to-NNE shearing event (64±4 Ma, Hansman et al., 2018), marking the time of deepest burial and measured in bedding parallel veins, were reconstructed to 186-221 °C by Holland et al. (2009) assuming an ophiolitic overburden of 5 km (Sahtan Fm., Wadi Nakhr). If we adjust this pressure correction for higher values of 280 to 340 MPa accounting for the here elaborated 8 to 10 km of ophiolite and 2 km of sedimentary nappes, trapping temperatures would increase to c. 296-364 °C (Table 3), which are in the order of the maximum burial temperatures as deduced from organic matter maturity.

Figure 11 presents a summary burial plot indicating temperature and age constraints. Highlighted in gray is additional information gained by fluid inclusion thermometry. These data indicate paleo-fluid temperatures in the range of 225 ± 4 (280 MPa) to 266 ± 5 °C (340 MPa) during burial under the ophiolite (bedding-confined veins), c. 296-364 °C at peak burial (top-to-NNE sheared veins) and 213 ± 3 °C during exhumation with a later phase of primary inclusion outlining 184 ± 3 to 189 ± 7 °C (both strike-slip related veins). Temperature decrease within the latter formed parts of the strike-slip veins might relate to a change of fluid source or to exhumation during vein formation. In combination with our thermochronology data the second possibility appears more likely and would imply strike-slip faults developed after c. 55 Ma.

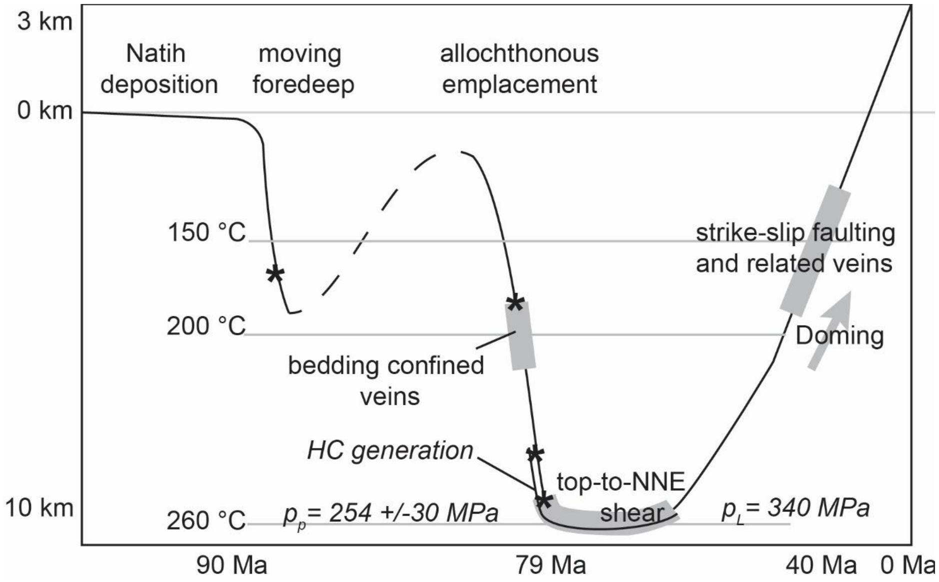

Figure 11: Summary burial sketch for the top of the carbonate platform (Natih Fm.). Shown temperatures are based on RSCM and FI thermometry, pressure data calculated out of FI measurements and independently determined temperature data. The uplift history is restored by ZHe ages. (* indicate times of overpressure formation, gray areas depict vein formation)

5.2. Exhumation history

Our new thermochronology data from the central part of the Jebel Akhdar Dome suggests cooling below the reset temperature of the ZHe thermochronometer (c. 170 °C) between 48.7 ± 1.8 and 39.8 ± 3.0 Ma (Table2, Figure 4). The small variation in cooling ages for the different stratigraphic levels indicates rapid passage of the entire rock suite through the ZHe partial retention zone, and consequently rapid exhumation of the Jebel Akhdar Dome. This Eocene cooling is in agreement with ZHe ages of pre-Permian strata of Hansman et al. (2017) ranging between 62 ± 3 and 39 ± 2 Ma. Apatite fission track (AFT) ages measured in the basement of the Jebel Akhdar range between 55 ± 5 Ma and 48 ± 7 Ma (4 samples, Poupeau et al. 1998) and 51 ± 8 Ma to 32 ± 4 Ma (Hansman et al., 2017). The temperature of resetting the AFT system (i.e. the depth of the base of the partial annealing zone) may vary depending on annealing kinetics. For different apatite crystals this temperature ranges between 100 and 120 °C (Carlson et al., 1999; Fitzgerald et al., 2006). Hence, these AFT ages reproduce within error with our ZHe results, despites the fact that both systems are sensitive to different temperature intervals (100-120 °C and 130-170 °C, respectively). This supports the interpretation of rapid exhumation of the Jebel Akhdar. In combination with zircon fission track ages of Saddiqi et al. (2006), indicating the rocks cooled below c. 260 °C between 70 and 96 Ma, modeled cooling paths indicate rapid exhumation initiated at c. 55 Ma. Earlier exhumation would not result in required thermal maturities as exposure of the rock to highest temperatures would be too short for thermal equilibration. A reheating event in the late Miocene is not required to explain the data.

Our ZHe data from the Muti Formation and the Hawasina Nappes show a spread in ages, ranging from 43 to 173 Ma, i.e. partly much older than the ages observed in the stratigraphically lower units in the center of the dome. This indicates the system has been only partially reset, implying these units were not heated above 170 °C after deposition. Units exposed in the Hawasina Window (Figure 1) also show unreset ZHe ages (Csontos, pers. comm.). The top of the Natih Formation has seen temperatures above 220 °C. We suggest this apparent contradiction may be explained by juxtaposition of the colder Muti and Hawasina units against the top of the carbonate platform during extensional top-to-NNE shearing. This implies that at least 50 °C of cooling are associated with post obduction extension, i.e. before doming. A two-stage exhumation history of the Jebel Akhdar Dome has also been inferred from structural data (Grobe et al., 2018; Mattern and Scharf, 2018) and the stratigraphic record (Fournier et al., 2006; Mann et al., 1990).

5.3. Pressure evolution and fluid migration

Evolution of pore pressures was modelled (Figures S6 and S7**Fehler! Verweisquelle konnte nicht gefunden werden.**) assuming a perfect seal on top of the Natih Fm. ($k_{Muti}=10^{-23}$ m^2). Porosity was lost during Muti deposition in the moving forebulge (top seal) and related burial, the emplacement of the Hawasina Nappes and the ophiolite, which induced compaction and a remaining very low porosity of c. 1 %. Hydrostatic pressure increased with the moving forebulge at 88 Ma to 40 MPa, after Muti deposition to 60 MPa and after ophiolite emplacement to 120 MPa. Calculated pore pressure exceeded hydrostatic pressure in response to Hawasina Nappe and ophiolite emplacement.

Formation of tensile fractures, as inferred from bedding confined, Mode-I veins in the Natih Fm.(Grobe et al., 2018; e.g. Holland et al., 2009; Virgo, 2015), require internal fluid pressures (P_f) exceeding the sum of the stress acting normal on the fracture surface (σ_3) and the tensile stress of the rock (T): $P_f > \sigma_3 + T$, and a differential stress (σ_1 - σ_3) below 4T (Secor, 1965). Host-rock buffered vein isotope compositions indicate that the veins were formed by local fluids (Arndt et al., 2014) and, hence, require local overpressure cells.

Sensitivity analyses of reduced permeabilities of Muti, Natih and Nahr Umr formations show that overpressure generation, necessary for rock fracturing, requires a very good top seal and a reduced horizontal permeability of the Natih Fm. of 10^{-23} m² (Figure S7). A top seal on its own is not sufficient for overpressures initiating rock failure. This case results in pore pressures up to 300 MPa within the top Natih and localized overpressures of 195 MPa in front of the obducting ophiolite.

All results indicate that without low horizontal permeabilities of the Natih Fm. $\leq 10^{-23}$ m² overpressure cells required for vein formation cannot be generated. The reduced permeabilities in the Natih Fm. are necessary to prevent an early, tectonically-driven horizontal pressure release.

5.4. Fluid migration

Numerical basin modeling shows that rapid burial of sedimentary rocks below the ophiolite (88-80 Ma) caused under-compaction, i.e. a porosity too high with respect to burial depth, and consequent pore pressure increase. Two example model results of fluid migration in front of the obducting ophiolite are shown in the electronic supplement Figure S8. If low permeabilities are assigned to the non-source-rock members of the Natih Fm., migration will mainly take place within the source rocks and at layer interfaces within the Natih Fm. If the complete Natih Fm. has low permeabilities, fluids will leave the source rock vertically first, before lateral migration localizes along layer boundaries. The pressure gradient between overpressures below the allochthonous nappes and the less deeply buried southern foreland initiates tectonically-driven fluid migration in front of the obducting nappes, an idea that was first introduced by Oliver (1986). Solid bitumen accumulations in black stained calcite veins are in agreement with this interpretation (Fink et al., 2015).

Dome formation of the Jebel Akhdar anticline around 55 Ma initiated layer tilting and consequent northward migration of the generated hydrocarbons as observed by secondary low reflective solid bitumen generations in Natih veins and host rocks at the southern flank of the Oman Mountains (Fink et al., 2015; Grobe et al., 2016).

6. Conclusions

This study provides insights into the temperature evolution during obduction, prior to subsequent orogenesis.

Arabia's passive continental margin was buried to at least 4 km at times of foredeep migration and afterwards under 8-10 km of Semail Ophiolite and 2 km of sedimentary Hawasina Nappes. Burial under the ophiolite resulted in peak temperatures of up to 300 °C (Shu'aiba Fm.) with sub-lithostatic pore pressures. Ophiolite obduction and overpressure cells expelled fluids towards the foreland, through matrix and fracture porosity.

ZHe data show cooling associated with forebulge migration, as well as with exhumation of the Jebel Akhdar Dome. Exhumation of the Jebel Akhdar Dome took place in two stages. A first stage is associated with top-to-NNE shearing, which is responsible for at least 50 °C of cooling, as witnessed by juxtaposition of units including partially reset ZHe ages against units that experienced more than 220 °C. ZHe data show the second exhumation phase, associated with doming of the Jebel Akhdar occurred between 49 and 39 Ma.

Author contribution

JLU, RL and AG conceived of the study. AG planned and carried out fieldwork as well as thermal maturity measurements (VR, solid bitumen reflectance, Raman spectroscopy), structural interpretations and basin modelling. CvH, JU and FW carried out fieldwork and structural interpretations. FW and ID conducted the thermochronological measurements with help of CvH. PM and AG performed fluid inclusion thermometry. AG and CvH prepared the manuscript with contributions from all co-authors.

Acknowledgements

We acknowledge the highly-appreciated help of Donka Macherey (sample preparation, RWTH Aachen), the team of the KU Leuven (fluid inclusion measurements) and Keno Lünsdorf (Raman spectroscopy, Georg-August-University, Göttingen). Sample crushing was realized by the team of SELFRAG, Switzerland. Wiekert Visser and Victoria Sachse are thanked for fruitful discussions; Gösta Hoffmann and Wilfried Bauer thanked for helping with field logistics. We are grateful for comments of Edwin Gnos, Andreas Scharf, Bruce Levell, Wolf-Christian Dullo and Mark Handy on earlier versions of this manuscript.

References

Agard, P., Omrani, J., Jolivet, L. and Mouthereau, F.: Convergence history across Zagros (Iran): constraints from collisional and earlier deformation, International Journal of Earth Sciences, 94(3), 401–419, doi:10.1007/s00531-005-0481-4, 2005.

Al-Kindi, M. H. and Richard, P. D.: The main structural styles of the hydrocarbon reservoirs in Oman, Geological Society, London, Special Publications, 392(1), 409–445, doi:10.1144/SP392.20, 2014.

Al-Lazki, A. I., Seber, D., Sandvol, E. and Barazangi, M.: A crustal transect across the Oman Mountains on the eastern margin of Arabia, GeoArabia, 7(1), 47–78, 2002.

Al-Wardi, M. and Butler, R. W. H.: Constrictional extensional tectonics in the northern Oman mountains, its role in culmination development and the exhumation of the subducted Arabian continental margin, Geological Society, London, Special Publication, 272(1), 187–202, doi:10.1144/GSL.SP.2007.272.01.11, 2007.

Aldega, L., Carminati, E., Scharf, A., Mattern, F. and Al-Wardi, M.: Estimating original thickness and extent of the Semail Ophiolite in the eastern Oman Mountains by paleothermal indicators, Marine and Petroleum Geology, 84, 18–33, doi:10.1016/j.marpetgeo.2017.03.024, 2017.

Aoya, M., Kouketsu, Y., Endo, S., Shimizu, H., Mizukami, T., Nakamura, D. and Wallis, S.: Extending the applicability of the Raman carbonaceous-material geothermometer using data from contact metamorphic rocks, Journal of Metamorphic Geology, 28(9), 895–914, doi:10.1111/j.1525-1314.2010.00896.x, 2010.

Arndt, M., Virgo, S., Cox, S. F. and Urai, J. L.: Changes in fluid pathways in a calcite vein mesh (Natih Fm, Oman Mountains): insights from stable isotopes, Geofluids, 14(4), 391–418, doi:10.1111/gfl.12083, 2014.

Barker, C. E. E. and Pawlewicz, M. J. J.: Calculation of vitrinite reflectance from thermal histories and peak temperatures, in Vitrinite Reflectance as a Maturity Parameter, vol. 570, edited by P. Mukhopadhyay and W. Dow, pp. 216–229, American Chemical Society., 1994.

Béchennec, F., Metour, J. L. E., Rabu, D., Villey, M. and Beurrier, M.: The Hawasina Basin: A fragment of a starved passive continental margin, thrust over the Arabian Platform during obduction of the Sumail Nappe, Tectonophysics, 151(1–4), 323–343, doi:10.1016/0040-1951(88)90251-X, 1988.

Béchennec, F., Le Metour, J., Rabu, D., Bourdillon-de-Grissac, C., de Wever, P., Beurrier, M. and Villey, M.: The Hawasina Nappes: stratigraphy, palaeogeography and structural evolution of a fragment of the south-Tethyan passive continental margin, Geological Society, London, Special Publications, 49(1), 213–223, doi:10.1144/GSL.SP.1992.049.01.14, 1990.

Bernoulli, D., Weissert, H. and Blome, C. D.: Evolution of the Triassic Hawasina Basin, Central Oman Mountains, Geological Society, London, Special Publications, 49(1), 189–202, doi:10.1144/GSL.SP.1992.049.01.12, 1990.

Beurrier, M., Bechennec, F., Rabu, D. and Hutin, G.: Geological Map of Rustaq - explanatory notes, Sultanat of Oman, Ministry of Petroleum and Minerals, 1986.

Beyssac, O., Goffé, B., Chopin, C. and Rouzaud, J. N.: Raman spectra of carbonaceous material in metasediments: A new geothermometer, Journal of Metamorphic Geology, 20, 859–871, doi:10.1046/j.1525-1314.2002.00408.x, 2002.

Bodnar, R. J.: Revised equation and table for determining the freezing point depression of H2O-NaCl solutions, Gechimica et Cosmochimica Acta, 57, 683–684, 1993.

Breton, J. P., Béchennec, F., Le Métour, J., Moen-Maurel, L. and Razin, P.: Eoalpine (Cretaceous) evolution of the Oman Tethyan continental margin: Insights from a structural field study in Jabal Akhdar (Oman Mountains), GeoArabia, 9(2), 41–58, 2004.

Brown, P. E.: FLINCOR; a microcomputer program for the reduction and investigation of fluid-inclusion data, American Mineralogist, 74, 1390–1393, 1989.

Van Buchem, F. S. P., Razin, P., Homewood, P. W., Philip, J. M., Eberli, G. P., Platel, J. P., Roger, J., Eschard, R., Desaubliaux, G. M. J., Boisseau, T., Leduc, J. P., Labourdette, R. and Cantaloube, S.: High resolution sequence stratigraphy of the Natih Formation (Cenomanian/Turonian) in northern Oman: distribution of source rocks and reservoir facies, GeoArabia, 1(1), 65–91, 1996.

Van Buchem, F. S. P., Razin, P., Homewood, P. W., Oterdoom, W. H. and Philip, J.: Stratigraphic organization of carbonate ramps and organic- rich intrashelf basins: Natih Formation (middle Cretaceous) of northern Oman, AAPG Bulletin, 86(1), 21–53, doi:10.1306/61EEDA30-173E-11D7-8645000102C1865D, 2002.

Carlson, W. D., Donelick, R. A. and Ketcham, R. A.: Variability of apatite fission-track annealing kinetics: I. Experimental results, American Mineralogist, 84(9), 1213–1223, doi:10.2138/am-1999-0901, 1999.

Claringbould, J. S., Hyden, B. B., Sarg, J. F. and Trudgill, B. D.: Structural evolution of a salt-cored, domed, reactivated fault complex, Jebel Madar, Oman, Journal of Structural Geology, 51, 118–131, doi:10.1016/j.jsg.2013.03.001, 2013.

Coleman, R. G.: Tectonic Setting for Ophiolite Obduction in Oman, Journal of Geophysical Research, 86(B4), 2497–2508, 1981.

Cooper, D. J. W., Ali, M. Y. and Searle, M. P.: Structure of the northern Oman Mountains from the Semail Ophiolite to the Foreland Basin, Geological Society, London, Special Publications, 392, 129–153, 2014.

Cowan, R. J., Searle, M. P. and Waters, D. J.: Structure of the metamorphic sole to the Oman Ophiolite, Sumeini Window and Wadi Tayyin: implications for ophiolite obduction processes, Geological Society, London, Special Publications, 392(1), 155–175, doi:10.1144/SP392.8, 2014.

Deville, E. and Sassi, W.: Contrasting thermal evolution of thrust systems: An analytical and modeling approach in the front of the western Alps, AAPG Bulletin, 90(6), 887–907, doi:10.1306/01090605046, 2006.

Duretz, T., Agard, P., Yamato, P., Ducassou, C. C., Burov, E. B. and Gerya, T. V.: Thermo-mechanical modeling of the obduction process based on the Oman Ophiolite case, Gondwana Research, doi:10.1016/j.gr.2015.02.002, 2015.

Ferreiro Mählmann, R.: Correlation of very low grade data to calibrate a thermal maturity model in a nappe tectonic setting, a case study from the Alps, Tectonophysics, 334, 1–33, 2001.

Filbrandt, J. B., Al-Dhahab, S., Al-Habsy, A., Harris, K., Keating, J., Al-mahruqi, S., Ozkaya, S. I., Richard, P. D. and Robertson, T.: Kinematic interpretation and structural evolution of North Oman, Block 6, since the Late Cretaceous and implications for timing of hydrocarbon migration into Cretaceous reservoirs, GeoArabia, 11(1), 97–115, 2006.

Fink, R., Virgo, S., Arndt, M., Visser, W., Littke, R. and Urai, J. L. L.: Solid bitumen in calcite veins from the Natih Formation in the Oman Mountains: Multiple phases of petroleum migration in a changing stress field, International Journal of Coal Geology, 157, 39–51, doi:10.1016/j.coal.2015.07.012, 2015.

Fitzgerald, P. G., Baldwin, S. L., Webb, L. E. and O'Sullivan, P. .: He data from slowly cooled crustal terranes and the interpretation of intra-sample variations of single crystal apatite ages from vertical profiles., Chemical Geology, 225, 91–120, 2006.

Forbes, G. A., Jansen, H. S. M. and Schreurs, J.: Lexicon of Oman - Subsurface Stratigraphy - Reference Guide to the Stratigraphy of Oman's Hydrocarbon Basins, GeoArabia special publication 5, 2010.

Fournier, M., Lepvrier, C., Razin, P. and Jolivet, L.: Late Cretaceous to Paleogene post-obduction extension and subsequent Neogene compression in the Oman Mountains, GeoArabia, 11(4), 17–40, 2006.

Glennie, K. W., Boeuf, M. G. A., Clarke, M. W. H., Moody-Stuart, M., Pilaar, W. F. H. and Reinhardt, B. M.: Late Cretaceous Nappes in Oman Mountains and Their Geologic Evolution, AAPG Bulletin, 57(1), 5–27, 1973.

Glennie, K. W., Boeuf, M. G. A., Hughes Clarke, M. W., Moody-Stuart, M., Pilaar, W. F. H. and Reinhardt, B. M.: Geology of the Oman Mountains, Verhandelingen van het Koninklijk Nederlands geologisch mijnbouwkundig Genootschap, 31, 432, 1974.

Gnos, E. and Peters, T.: K-Ar ages of the metamorphic sole of the Semail Ophiolite: implications for ophiolite cooling history, Contributions to Mineralogy and Petrology, 113, 325–332, 1993.

Goldstein, R. H.: Fluid inclusions in sedimentary and diagenetic systems, Lithos, 55(1–4), 159–193, doi:10.1016/S0024-4937(00)00044-X, 2001.

Gomez-Rivas, E., Bons, P. D., Koehn, D., Urai, J. L., Arndt, M., Virgo, S., Laurich, B., Zeeb, C., Stark, L. and Blum, P.: The Jabal Akhdar Dome in the Oman mountains: Evolution of a dynamic fracture system, American Journal of Science, 314(7), 1104–1139, doi:10.2475/07.2014.02, 2014.

Grelaud, C., Razin, P., Homewood, P. W. and Schwab, a. M.: Development of Incisions on a Periodically Emergent Carbonate Platform (Natih Formation, Late Cretaceous, Oman), Journal of Sedimentary Research, 76(4), 647–669, doi:10.2110/jsr.2006.058, 2006.

Grobe, A., Littke, R., Urai, J. L. and Lünsdorf, N. K.: Hydrocarbon generation and migration under a large overthrust: The carbonate platform under the Semail Ophiolite, Jebel Akhdar, Oman, International Journal of Coal Geology, 168, 3–19, doi:10.1016/j.coal.2016.02.007, 2016.

Grobe, A., Virgo, S., von Hagke, C., Urai, J. L. and Littke, R.: Multiphase Structural Evolution of a Continental Margin During Obduction Orogeny: Insights From the Jebel Akhdar Dome, Oman Mountains, Tectonics, 37(3), 888–913, doi:10.1002/2016TC004442, 2018.

Guenther, W. R., Reiners, P. W., Ketcham, R. A., Nasdala, L. and Giester, G.: American Journal of Science, American Journal of Science, 313(March), 145–198, doi:10.2475/03.2013.01, 2013.

Habsi, N. Al, Shukaili, M. Al, Tooqi, S. Al, Ehrenberg, S. N. and Bernecker, M.: Lithofacies, diagenesis and reservoir quality of Upper Shu'aiba reservoirs in northwestern Oman, GeoArabia, 19(4), 145–182, 2014.

Hacker, B. R. and Mosenfelder, J. L.: Metamorphism and deformation along the emplacement thrust of the Samail ophiolite, Oman, Earth and Planetary Science Letters, 144(3–4), 435–451, doi:10.1016/S0012-821X(96)00186-0, 1996.

Hacker, B. R., Mosenfelder, J. L. and Gnos, E.: Rapid emplacement of the Oman ophiolite: Thermal and geochronologic constraints, Tectonics, 15(6), 1230–1247, 1996.

Hanna, S. S.: The Alpine deformation of the Central Oman Mountains, Geological Society, London, Special Publications, 49(1), 341–359, doi:10.1144/GSL.SP.1992.049.01.21, 1990.

Hansman, R. J., Ring, U., Thomson, S. N. and Brok, B. Den: Late Eocene uplift of the Al Hajar Mountains, Oman, supported by stratigraphy and low-temperature thermochronology, Tectonics, doi:10.1002/2017TC004672, 2017.

Hansman, R. J., Albert, R., Gerdes, A. and Ring, U.: Absolute ages of multiple generations of brittle structures by U-Pb dating of calcite, Geology, doi:10.1130/G39822.1, 2018.

Hassanzadeh, J. and Wernicke, B. P.: The Neotethyan Sanandaj-Sirjan zone of Iran as an archetype for passive margin-arc transitions, Tectonics, 25(3), 586–621, doi:10.1002/2015TC003926, 2016.

Hilgers, C., Kirschner, D. L., Breton, J. P. P. and Urai, J. L.: Fracture sealing and fluid overpressures in limestones of the Jabal Akhdar dome, Oman mountains, Geofluids, 6(2), 168–184, doi:10.1111/j.1468-8123.2006.00141.x, 2006.

Hillier, S., Mátyás, J., Matter, A. and Vasseur, G.: Illite/smectite diagenesis and its variable correlation with vitrinite reflectance in the Pannonian Basin, Clays and Clay Minerals, 43(2), 174–183, doi:10.1346/CCMN.1995.0430204, 1995.

Holland, M., Urai, J. L., Muchez, P. and Willemse, E. J. M.: Evolution of fractures in a highly dynamic thermal, hydraulic, and mechanical system - (I) Field observations in Mesozoic Carbonates, Jabal Shams, Oman Mountains, GeoArabia, 14(1), 57–110, 2009.

Homewood, P., Razin, P., Grélaud, C., Droste, H., Vahrenkamp, V., Mettraux, M. and Mattner, J.: Outcrop sedimentology of the Natih Formation, northern Oman: A field guide to selected outcrops in the Adam Foothills and Al Jabal al Akhdar areas, GeoArabia, 13(3), 39–120, 2008.

Immenhauser, A. and Scott, R. W.: An estimate of Albian sea-level amplitudes and its implication for the duration of stratigraphic hiatuses, Sedimentary Geology, 152(1–2), 19–28, doi:10.1016/S0037-0738(02)00260-9, 2002.

Immenhauser, A., Schlager, W., Burns, S. J., Scott, R. W., Geel, T., Lehmann, J., van der Gaast, S. and Bolder-Schrijver, L. J. A. J. a.: Late Aptian to late Albian sea-level fluctuations constrained by geochemical and biological evidence (Nahr Umr Formation, Oman), Journal of Sedimentary Research, 69(2), 434–446, doi:10.2110/jsr.69.434, 1999.

Jacobs, J., Thomas, R. J., Ksienzyk, A. K. and Dunkl, I.: Tracking the Oman Ophiolite to the surface - New fission track and (U-Th)/He data from the Aswad and Khor Fakkan Blocks, UAE, Tectonophysics, 644, 68–80, doi:10.1016/j.tecto.2014.12.018, 2015.

De Keijzer, M., Hillgartner, H., Al Dhahab, S. and Rawnsley, K.: A surface-subsurface study of reservoir-scale fracture heterogeneities in Cretaceous carbonates, North Oman, Geological Society, London, Special Publications, 270(1), 227–244, doi:10.1144/GSL.SP.2007.270.01.15, 2007.

Ketcham, R. A.: Forward and Inverse Modeling of Low-Temperature Thermochronometry Data, Reviews in Mineralogy and Geochemistry, 58, 275–314, doi:10.2138/rmg.2005.58.11, 2005.

Koehrer, B., Zeller, M., Aigner, T., Poeppelreiter, M., Milroy, P., Forke, H. and Al-Kindi, S.: Facies and stratigraphic framework of a Khuff outcrop equivalent: Saiq and Mahil formations, Al Jabal al-Akhdar, Sultanate of Oman, GeoArabia, 15(2), 91–156, 2010.

Koehrer, B., Aigner, T. and Poppelreiter, M.: Field-scale geometries of Upper Khuff reservoir geobodies in an outcrop analogue (Oman Mountains, Sultanate of Oman), Petroleum Geoscience, 17(1), 3–16, doi:10.1144/1354-079310-009, 2011.

Kouketsu, Y., Mizukami, T., Mori, H., Endo, S., Aoya, M., Hara, H., Nakamura, D. and Wallis, S.: A new approach to develop the Raman carbonaceous material geothermometer for low-grade metamorphism using peak width, Island Arc, 23, 33–50, doi:10.1111/iar.12057, 2014.

Lippard, S. J., Smewing, J. D., Rothery, D. a. and Browning, P.: The geology of the Dibba zone, northern Oman mountains - a preliminary study, Journal of the Geological Society, 139(1), 59–66, doi:10.1144/gsjgs.139.1.0059, 1982.

Loosveld, R. J. H., Bell, A. and Terken, J. J. M.: The Tectonic Evolution of Interior Oman, GeoArabia, 1(1), 28–51, 1996.

Lünsdorf, N. K.: Raman spectroscopy of dispersed vitrinite - methodical aspects and correlation with reflectance, International Journal of Coal Geology, 153(1), 75–86, doi:10.1016/j.coal.2015.11.010, 2016.

Lünsdorf, N. K., Dunkl, I., Schmidt, B. C., Rantitsch, G. and von Eynatten, H.: The thermal history of the Steinach Nappe (eastern Alps) during extension along the Brenner Normal Fault system indicated by organic maturation and zircon (U-Th)/ He thermochronology, Austrian Journal of Earth Sciences, 105(3), 17–25, 2012.

Lutz, R., Littke, R., Gerling, P. and Bönnemann, C.: 2D numerical modelling of hydrocarbon generation in subducted sediments at the active continental margin of Costa Rica, Marine and Petroleum Geology, 21(6), 753–766, doi:10.1016/j.marpetgeo.2004.03.005, 2004.

Mann, a., Hanna, S. S. and Nolan, S. C.: The post-Campanian tectonic evolution of the Central Oman Mountains: Tertiary extension of the Eastern Arabian Margin, The Geology and Tectonics of the Oman Region, 49(1), 549–563, doi:10.1144/gsl.sp.1992.049.01.33, 1990.

Mattern, F. and Scharf, A.: Postobductional extension along and within the Frontal Range of the Eastern Oman Mountains, Journal of Asian Earth Sciences2, 154, doi:10.1016/j.jseaes.2017.12.031, 2018.

Le Metour, J., Rabu, D., Tegyey, M., Bechennec, F., Beurrier, M. and Villey, M.: Subduction and obduction: two stages in the EoAlpine tectonometamorphic evolution of the Oman Mountains, Geological Society, London, Special Publications, 49(1), 327–339, doi:10.1144/GSL.SP.1992.049.01.20, 1990.

Mount, V. S., Crawford, R. I. S., Bergmann, S. C. and Bergman, S. C.: Regional Structural Style of the Central and Southern Oman Mountains: Jebel Akhdar, Saih Hatat, and the Northern Ghaba Basin, GeoArabia, 3(4), 17, 1998.

Mouthereau, F.: Timing of uplift in the Zagros belt/Iranian plateau and accommodation of late Cenozoic Arabia - Eurasia convergence, Geological Magazine, 148(5–6), 726–738, doi:10.1017/S0016756811000306, 2011.

Mozafari, M., Swennen, R., Balsamo, F., Clemenzi, L., Storti, F., El Desouky, H., Vanhaecke, F., Tueckmantel, C., Solum, J. and Taberner, C.: Paleofluid Evolution In Fault-Damage Zones: Evidence From Fault-Fold Interaction Events In the Jabal Qusaybah Anticline (Adam Foothills, North Oman), Journal of Sedimentary Research, 85(12), 1525–1551, doi:10.2110/jsr.2015.95, 2015.

Muchez, P., Marshall, J. D., Touret, J. L. R. and Viaene, W. a.: Origin and migration of palaeofluids in the Upper Visean of the Campine Basin, northern Belgium, Sedimentology, 41(1), 133–145, doi:10.1111/j.1365-

3091.1994.tb01395.x, 1994.

Neumaier, M.: Structural Restoration and Basin and Petroleum Systems Modeling: Case Studies from the Monagas Fold and Thrust Belt, Venezuela and the Moroccan Atlantic Margin, Dissertation, RWTH Aachen University., 2015.

Nolan, S. C., Skelton, P. W., Clissold, B. P. and Smewing, J. D.: Maastrichtian to early Tertiary stratigraphy and palaeogeography of the Central and Northern Oman Mountains, Geological Society, London, Special Publications, 49(1), 495–519, doi:10.1144/gsl.sp.1992.049.01.31, 1990.

Nöth, S., Karg, H. and Littke, R.: Reconstruction of Late Paleozoic heat flows and burial histories at the Rhenohercynian-Subvariscan boundary, Germany, International Journal of Earth Sciences, 90(2), 234–256, doi:10.1007/s005310000114, 2001.

Oliver, J.: Fluids expelled tectonically from orogenic belts: Their role in hydrocarbon migration and other geologic phenomena, Geology, 14(February), 99–102, 1986.

Oxburgh, E. R. and Turcotte, D. L.: Thermal gradients and regional metamorphism in overthrust terrains with special reference to the Eastern Alps, Schweizerische Mineralogische und Petrographische Mitteilungen, 54(2/3), 642–662, 1974.

Philip, J., Borgomano, J. and Al-Maskiry, S.: Cenomanian-Early Turonian carbonate platform of Northern Oman: stratigraphy and palaeo-environments, Palaeogeography, Palaeoclimatology, Palaeoecology, 119, 77–92, 1995.

Pöppelreiter, M. C., Schneider, C. J., Obermaier, M., Forke, H. C., Koehrer, B. and Aigner, T.: Seal turns into reservoir: Sudair equivalents in outcrops, A1 Jabal al-Akhdar, Sultanate of Oman, GeoArabia, 16(1), 69–108, 2011.

Poupeau, G., Saddiqi, O., Michard, A., Goffé, B. and Oberhänsli, R.: Late thermal evolution of the Oman Mountains subophiolitic windows: Apatite fission-track thermochronology, Geology, 26(12), 1139–1142, 1998.

Pratt, R., Smewing, D., Swansea, S. A., Pratt, B. R. and Smewing, J. D.: Jurassic and Early Cretaceous platform margin configuration and evolution, central Oman Mountains, Geological Society, London, Special Publications, 49(1), 69–88, doi:10.1144/GSL.SP.1992.049.01.06, 1990.

Rabu, D., Le Metour, J., Bechennec, F., Beurrier, M., Villey, M. and Bourdillon-Jeudy de Grissac, C.: Sedimentary aspects of the Eo-Alpine cycle on the northeast edge of the Arabian Platform (Oman Mountains), Geological Society, London, Special Publications, 49(1), 49–68, doi:10.1144/GSL.SP.1992.049.01.05, 1990.

Rantitsch, G. and Rainer, T.: Thermal modeling of Carboniferous to Triassic sediments of the Karawanken Range (Southern Alps) as a tool for paleogeographic reconstructions in the Alpine-Dinaridic-Pannonian realm, International Journal of Earth Sciences, 92(2), 195–209, doi:10.1007/s00531-003-0312-4, 2003.

Reiners, P. W.: Zircon (U-Th)/He Thermochronometry, Reviews in Mineralogy and Geochemistry, 58(1936), 151–179, doi:10.2138/rmg.2005.58.6, 2005.

Reutter, K.-J., Teichmüller, M. and Teichmüller, R.: The Coalification Pattern in the Northern Apennines and its Palaeogeothermic and Tectonic Significance, Geologische RundschauGeologische Rundschau, 72(3), 861–894, 1988.

Rioux, M., Bowring, S., Kelemen, P., Gordon, S., Miller, R. and Dudás, F.: Tectonic development of the Samail ophiolite: High-precision U-Pb zircon geochronology and Sm-Nd isotopic constraints on crustal growth and emplacement, Journal of Geophysical Research: Solid Earth, 118(5), 2085–2101, doi:10.1002/jgrb.50139, 2013.

Rioux, M., Garber, J., Bauer, A., Bowring, S., Searle, M., Kelemen, P. and Hacker, B.: Synchronous formation of the metamorphic sole and igneous crust of the Semail ophiolite: New constraints on the tectonic evolution during ophiolite formation from high-precision U–Pb zircon geochronology, Earth and Planetary Science Letters, 451, 185–195, doi:10.1016/j.epsl.2016.06.051, 2016.

Robertson, A.: The transition from a passive margin to an Upper Cretaceous foreland basin related to ophiolite emplacement in the Oman Mountains, Geological Society of America Bulletin, 99, 633–653, doi:10.1130/0016-7606(1987)99<633, 1987.

Rolandone, F., Lucazeau, F., Leroy, S., Mareschal, J.-C., Jorand, R., Goutorbe, B. and Bouquerel, H.: New heat flow measurements in Oman and the thermal state of the Arabian Shield and Platform, Tectonophysics, 589, 77–89, doi:10.1016/j.tecto.2012.12.034, 2013.

Roure, F., Andriessen, P., Callot, J. P., Faure, J. L., Ferket, H., Gonzales, E., Guilhaumou, N., Lacombe, O., Malandain, J., Sassi, W., Schneider, F., Swennen, R. and Vilasi, N.: The use of palaeo-thermo-barometers and coupled thermal, fluid flow and pore-fluid pressure modelling for hydrocarbon and reservoir prediction in fold and thrust belts, Geological Society, London, Special Publications, 348(1), 87–114, doi:10.1144/SP348.6, 2010.

Saddiqi, O., Michard, A. N., Goffe, B. R., Poupeau, G. É. and Oberhänsli, R. O.: Fission-track thermochronology of the Oman Mountains continental windows, and current problems of tectonic interpretation, Bull. Soc. géol. Fr., 177(3), 127–134, doi:10.2113/gssgfbull.177.3.127, 2006.

Scott, R. W.: Chronostratigraphy of the Cretaceous carbonate shelf, southeastern Arabia, Geological Society, London, Special Publications, 49(1), 89–108, doi:10.1144/GSL.SP.1992.049.01.07, 1990.

Searle, M. P.: Sequence of thrusting and origin of culminations in the northern and central Oman Mountains, Journal of Structural Geology, 7(2), 129–143, doi:10.1016/0191-8141(85)90127-0, 1985.

Searle, M. P.: Structural geometry, style and timing of deformation in the Hawasina Window, Al Jabal al Akhdar and Saih Hatat culminations, Oman Mountains, GeoArabia, 12(2), 99–130, 2007.

Searle, M. P. and Cox, J. O. N.: Subduction zone metamorphism during formation and emplacement of the Semail ophiolite in the Oman Mountains, Geological Magazine, 139(3), 241–255, doi:10.1017/S0016756802006532, 2002.

Searle, M. P., Warren, C. J., Waters, D. J. and Parrish, R. R.: Subduction zone polarity in the Oman Mountains: implications for ophiolite emplacement, Geological Society, London, Special Publications, 218(1), 467–480, doi:10.1144/GSL.SP.2003.218.01.24, 2003.

Searle, M. P., Warren, C. J. J., Waters, D. . J. and Parrish, R. . R.: Structural evolution, metamorphism and restoration of the Arabian continental margin, Saih Hatat region, Oman Mountains, Journal of Structural Geology, 26(3), 451–473, doi:10.1016/j.jsg.2003.08.005, 2004.

Secor, D. T. jr.: Role of fluid pressure in jointing, American Journal of Science, 263(October), 633–646, 1965.

Stenhouse, P.: Reactive Transport and Fluid Pathways in Fracture-Controlled Flow Systems, (Doctoral Dissertation)., Australian National University., 2014.

Sweeney, J. J. and Burnham, A. K.: Evaluation of a Simple Model of Vitrinite Reflectance Based on Chemical Kinetics, The American Association of Petroleum Geologists Bulletin, 74(10), 1559–1570, 1990.

Teichmüller, R. and Teichmüller, M.: Relations between coalification and palaeogeothermics in Variscan and Alpidic foredeeps of western Europe, Lecture Notes in Earth Sciences, 5, 1986.

Terken, J. M. J.: The Natih petroleum system of north Oman, GeoArabia, 4(2), 157–180, 1999.

Terken, J. M. J., Frewin, N. L., Indrelid, S. L. and Indrelin, S. L.: Petroleum systems of Oman: Charge timing and risks, AAPG Bulletin, 85(10), 1817–1845, 2001.

Vahrenkamp, V. C.: Chemostratigraphy of the Lower Cretaceous Shu'aiba Formation: A delta-13C reference profile for the Aptian Stage from the southern Neo-Tethys Ocean, GeoArabia, 1, 107–137, 2010.

Velde, B. and Lanson, B.: Comparison of I/S transformation and maturity of organic matter at elevated temperatures, Clays and Clay Minerals, 41(2), 178–183, 1993.

Virgo, S.: Aspects of crack-seal vein system evolution. (Doctoral Dissertation). Retrieved from http://nbn-resolving.de/urn/resolver.pl?urn=urn:nbn:de:hbz:82-opus-33858., RWTH Aachen University., 2015.

Virgo, S. and Arndt, M.: Evolution of a crack-seal calcite vein network in limestone: a high resolution structural, microstructural and geochemical study from the Jebel Akhdar high pressure cell, Oman Mountains, (Diploma Thesis)., RWTH Aachen [online] Available from: http://darwin.bth.rwth-aachen.de/opus3/volltexte/2010/3385/, 2010.

Virgo, S., Arndt, M., Sobisch, Z. Z. and Urai, J. L.: Development of fault and vein networks in a carbonate sequence near Hayl al-Shaz, Oman Mountains, GeoArabia, 18(2), 99–136 [online] Available from: http://www.gulfpetrolink.net/publication/vol18.php, 2013.

Visser, W.: Burial and thermal history of Proterozoic source rocks in Oman, Precambrian Research, 54(1), 15–36, doi:10.1016/0301-9268(91)90066-J, 1991.

Warburton, J., Burnhill, T. J., Graham, R. H. and Isaac, K. P.: The evolution of the Oman Mountains Foreland Basin, The Geology and Tectonics of the Oman Region, 49(1), 419–427, doi:10.1144/GSL.SP.1992.049.01.26, 1990.

Warren, C. J., Parrish, R. R., Searle, M. P. and Waters, D. J.: Dating the subduction of the Arabian continental margin beneath the Semail ophiolite, Oman, Geology, 31(10), 889, doi:10.1130/G19666.1, 2003.

Warren, C. J., Parrish, R. R., Waters, D. J. and Searle, M. P.: Dating the geologic history of Oman's Semail ophiolite: insights from U-Pb geochronology, Contributions to Mineralogy and Petrology, 150(4), 403–422, doi:10.1007/s00410-005-0028-5, 2005.

Wygrala, B. P.: Integrated study on an oil field in the southern po basin, northern italy, Berichte der Kernforschungsanlage Jülich, 2313(October), 217, 1989.